NASA TECHNICAL MEMORANDUM

NASA TM X- 72699

NASA TM X- 72699

(NASA-TM-X-72699) THE SELF STREAMLINING WIND TUNNEL (NASA) 45 p HC $3.75 CSCL 14B

N75-28080

Unclas
G3/09 31092

THE SELF STREAMLINING WIND TUNNEL

By Michael J. Goodyer

NATIONAL AERONAUTICS AND SPACE ADMINISTRATION
LANGLEY RESEARCH CENTER, HAMPTON, VIRGINIA 23665

1. Report No.	2. Government Accession No.	3. Recipient's Catalog No.
NASA TM X-72699		

4. Title and Subtitle	5. Report Date
The Self Streamlining Wind Tunnel	AUGUST 1975
	6. Performing Organization Code

7. Author(s)	8. Performing Organization Report No.
Michael J. Goodyer	
	10. Work Unit No.

9. Performing Organization Name and Address	11. Contract or Grant No.
The University of Southampton Southampton, England	
	13. Type of Report and Period Covered
12. Sponsoring Agency Name and Address	Technical Memorandum
National Aeronautics and Space Administration Washington, D. C. 20546	14. Sponsoring Agency Code

15. Supplementary Notes

Michael J. Goodyer is lecturer in the Department of Aeronautics and Astronautics, The University of Southampton, England.

16. Abstract

A two dimensional test section in a low speed wind tunnel is producing flow conditions free from wall interference. The test section has flexible top and bottom walls, and rigid sidewalls from which the models are mounted spanning the tunnel. All walls are unperforated, and the flexible walls are positioned by screw jacks. To eliminate wall interference, the wind tunnel itself supplies the information required in the streamlining process, when run with the model present. Measurements taken at the flexible walls are used by the tunnels computer to check wall contours. Suitable adjustments based on streamlining criteria are then suggested by the computer. The streamlining criterion adopted when generating infinite flowfield conditions is a matching of static pressures in the test section at a wall with pressures computed for an imaginary inviscid flowfield passing over the outside of the same wall. A series of iterations brings the walls from straight to streamlines. Aerodynamic data taken on a cylindrical model operating under high blockage conditions is presented to illustrate the operation of the tunnel in its various modes.

17. Key Words (Suggested by Author(s)) (STAR category underlined)	18. Distribution Statement
Facilities, research and support flexible-wall wind-tunnel	Unclassified-Unlimited

19. Security Classif. (of this report)	20. Security Classif. (of this page)	21. No. of Pages	22. Price*
Unclassified	Unclassified	23	$4.25

*Available from { The National Technical Information Service, Springfield, Virginia 22151
STIF/NASA Scientific and Technical Information Facility, P.O. Box 33, College Park, MD 20740

Contents.

NATIONAL AERONAUTICS AND SPACE ADMINISTRATION

THE SELF STREAMLINING WIND TUNNEL

By Michael John Goodyer
The University
Southampton
England

Summary.

A two dimensional test section in a low speed wind tunnel is producing flow conditions free from wall interference. The test section has flexible top and bottom walls, and rigid sidewalls from which the models are mounted spanning the tunnel. All walls are unperforated, and the flexible walls are positioned by screw jacks. To eliminate wall interference, the wind tunnel itself supplies the information required in the streamlining process, when run with the model present. Measurements taken at the flexible walls are used by the tunnels computer to check wall contours. Suitable adjustments based on streamlining criteria are then suggested by the computer. The streamlining criterion adopted when generating infinite flowfield conditions is a matching of static pressures in the test section at a wall with pressures computed for an imaginary inviscid flowfield passing over the outside of the same wall. A series of iterations brings the walls from straight to streamlines. Aerodynamic data taken on a cylindrical model operating under high blockage conditions is presented to illustrate the operation of the tunnel in its various modes.

1. Introduction.

The need for improved test environments for wind tunnel models has long been apparent from disparities between tunnel and flight data. The airflow past a model is not representative of flight for a number of reasons, included among which are aspects of the geometry of its environment which interfere with the flow over the model. The interference can create errors in observation which are beyond correction, and has several sources the most serious of which are the presence of model supports, and the presence of the test section walls. The object of the research work covered by this report was to devise and demonstrate means for the elimination of the latter source of interference, namely that which is introduced as a result of the finite size of the test section.

For the flight of an aircraft to be simulated properly in a wind tunnel test at speeds up to and including the transonic range, the flow over the model is required to match the flight values of Reynolds number, Mach number and steadiness, and behave in all cases (except where ground-proximity is being simulated) as though the model were in an infinite flowfield. This is because an aircraft disturbs air infinitely far from itself, and therefore proper model simulation requires that the air flowing around the model be allowed to be disturbed infinitely far away, otherwise the simulation is imperfect and the aerodynamic forces acting on the model will be wrong. The effect of the finite size of the test section can be divided into two forms: the effect of its finite extent upstream and downstream of the model, and the effect of the proximity of the walls.

The costs of wind tunnel construction and testing are not affected strongly by the provision of test sections which are long enough to reduce the interference effects of finite length to acceptably small values. However, the reverse is true of the second form of wall interference. In this case tunnel costs have played a dominant role, forcing the use of rather small test section cross-sectional areas such that not only does the proximity of the flow boundary interfere with the flow over the model, but also it forces the use of values of model Reynolds numbers well below flight values. Corrections are required

to the measured aerodynamic forces for these two effects, but it is now recognized that the corrections cannot always be made with sufficient accuracy. Therefore, it is necessary to reproduce more closely the full scale flows.

A further step towards the proper simulation of full scale flight conditions would be the removal of the interference of the model supports. One way in which this is achieved is by the magnetic suspension of the model, where the aerodynamic forces acting on the magnetised model are resisted by electro-magnets around the test section. For maximum force capability the magnets are positioned as closely as possible to the test-section walls. However, in the case of transonic testing where a plenum chamber surrounds the ventilated test section it may be necessary to position the magnets outside the plenum chamber rather than alongside the test section. The result would be a large reduction in the force and moment capabilities of the magnets, which would be countered by the use of larger and more costly magnets.

Since one object of the ventilated walls and plenum chamber is to allow streamlines near the test section wall to flow through the walls in order to generate streamline patterns representative of tests in an infinite flow field, it would be possible to avoid the need for ventilation altogether if the walls themselves were contoured such that they had the effective shape of a set of streamlines in an infinite field. In avoiding ventilation, the need for a plenum chamber is removed and degradation in electro-magnet performance is avoided. Historically this was the motivation for initiating work during the period that the author was a Post Doctoral Research Associate at the NASA Langley Research Center which led to the construction and commissioning at the University of Southampton in 1973 of a wind tunnel test section having flexible walls, walls which could be contoured into effective streamline shapes.

It was early apparent that there were several additional and equally important advantages to be gained from the successful development of such a testing technique:

i) in avoiding test section ventilation by porous or slotted walls, this source of flow unsteadiness would be removed.

ii) the elimination of plenum suction would reduce significantly the energy consumption and costs of transonic testing.

iii) in simulating an infinite flow-field, the need for wall interference corrections would be removed.

iv) with non-interfering walls, larger models relative to test section size could be used with the result that full-scale Reynolds numbers might be achieved more easily. In this way the need for Reynolds number corrections would be removed.

The concept of providing the test section with flexible walls is far from new. A notable example of the use of a pair of such walls in two-dimensional testing is given in reference 1, which describes a tunnel having a 20 inch x 8 inch test section which remained in service for about ten years. For this tunnel approximate rules were established for setting the walls to streamlines around a range of theoretical models, the models and flows being readily amenable to analysis. The same rules were used in practical wind tunnel tests. The setting technique which was chosen required the walls to be positioned to contours which gave a constant pressure along their lengths. The walls were then re-positioned to a setting about mid-way between this contour and the straight before test data was taken on the model. While the mechanical design of the test section employed in the present work is similar, the method for establishing streamline wall contours is fundamentally different. The method relies on the matching of the real flow inside the contoured test section with a theoretically determined imaginary flow over the outside of the same contour. It appears that the same notion had occurred quite independently to several other workers at around the same time, for example Rubbert of the Boeing Company described his studies to the author in July 1972 and papers have been published by Ferri[2] and Sears[3]. In fact, the principle is so simple and obvious that it is probably not original; it might just be that its exploitation was not feasible before computers became readily available. The principal differences between the various approaches currently advocated lies in the practical implementation of the notion. Sears[3] is developing a ventilated two-dimensional test section with provision for control over the flow through the walls along the length of the test section. In this way streamlines near to

the walls can be controlled to conform to streamlines in an infinite field. The method has the advantage in transonic testing that wave cancellation would be as good as in normal ventilated test sections.

In the case of the solid but flexible-walled test section described in this report, application to testing in flows where the Mach number at the walls never exceeds unity might be relatively straightforward. Evidence that the technique is successful and easy to apply to low speed testing is presented. However, the application of flexible walls to tests in the important regime where wave cancellation is necessary will require research effort beyond that covered in this report.

The preceeding discussion has centered on flow around a single model in an infinite flowfield. However, a flexible walled wind tunnel may be used in a much more general way than this. With a single model in the test section, an airfoil for example, the test section may be arranged to simulate:-

i) Conventional closed test section flow simulating approximately an infinite array of alternate images.

ii) Conventional open test-section flow.

iii) A single airfoil in an infinite flowfield.

iv) Dual mirror-image models in an infinite flowfield, simulating ground-effect.

v) An infinite cascade of identical airfoils.

In the next section a set of criteria is presented which ensure that the wall contours are those required for each mode. While the criteria advocated are general in that they can be applied to two- or three-dimensional testing, they will be illustrated with two-dimensional examples, where there are two walls to be contoured and these only in single curvature. Reference can then be made to contouring the walls to streamline shapes rather than, in the general case, of contouring to the surface of a streamtube.

There are of course an infinite number of shapes that can be adopted by a flexible wall. Therefore any criterion which is applied in choosing a contour must leave no residue of doubt about the correctness of the contour. It follows immediately that the criteria must be free from dependence on any assumptions about the nature of the flow over the model surface and in its vicinity.

The latter is based on the argument that if we could calculate or otherwise determine such flows with confidence there would be no need for wind tunnel tests.

The criteria are presented in the next section, followed by a description of a tunnel as modified for interference-free two-dimensional testing by the addition of a pair of flexible walls, and test data under various modes of operation.

2. Criteria For Correct Wall Streamlining.

2.1. Closed test section mode.

This is the mode of operation of many low speed and supersonic wind tunnels, where the walls generate approximately the flowfield of an infinite array of images. An illustration of two-dimensional wing testing is given on Fig. 1 (a), which also shows the nearest images.

The straight dividing streamlines between these images and the model coincide with the walls, and therefore the criterion for correct wall streamlining is simply that the walls are straight. Movement of the model vertically relative to the walls simply changes the image pattern.

In the case of a flexible walled test section the walls are adjusted for constant static pressure along their lengths with the test section empty. In this way allowance is made for the growth of the boundary layer displacement thickness along the tunnel walls. The change of displacement thickness in the presence of the model reduces the accuracy of interference corrections in conventional tunnels. The changes are allowed for in the setting of the flexible walls.

2.2. Open-jet mode.

Some aerodynamic testing is done in open-jets, where the boundary of the jet is subject to ambient pressure. This mode of model testing may be simulated in the self-streamlining tunnel by adjusting both flexible walls to contours which give static pressures everywhere along the walls constant and equal to ambient pressure. The setting of this contour was one step in the streamlining procedure suggested by Lock and Beavan[1]. The open-jet mode is

illustrated on Fig. 1 (b). The same airfoil is used throughout the sketches in Fig. 1, set at the same incidence. In Fig. 1 (b) there is a net turning of the flow passing the airfoil.

2.3. Infinite flowfield mode.

The flowfield around a two-dimensional wing in an infinite flowfield is illustrated schematically on Fig. 1 (c). The self-streamlining wind tunnel requires the flexible walls of its test section to follow streamlines above and below the airfoil. Two such streamlines are identified on the figure where they divide the flowfield into three portions, that above the top wall and extending upward to infinity, the real portion passing through the test section and over the airfoil, and the portion below the bottom wall extending downward to infinity. In the self-streamlining wind tunnel the portions of flowfield outside the walls are imaginary.

The criterion for correct wall streamlining in this case is illustrated by Fig. 2. Here a set of streamlines in an infinite flowfield is shown disturbed from the freestream direction by a model situated somewhere near the center of the diagram. A static pressure distribution is shown along the line XX cutting the streamlines. The distribution is continuous and therefore at any point in the flow the pressures each side of the streamline passing through that point are equal. For example, consider streamline S cutting XX at A. At this point the pressure P_r in the flow just below the streamline is equal to P_i just above. By similar reasoning $p_{i1} = P_{r1}$, $P_{i2} = P_{r2}$ etc. The streamline is not supporting a pressure difference.

Any convenient streamline such as SS may be chosen as a dividing streamline between the imaginary outer flow and the real flow inside the tunnel. The outer imaginary flow is completely potential provided that the dividing streamline does not penetrate the wake or boundary layer of the model, and therefore an inviscid solution to an imaginary field flowing over the contour SS is possible and proper, a rare event in fluid dynamics.

The matching of pressures P_i and P_r across a potential flow dividing streamline common to both the inner real flow and the outer imaginary flow is chosen as the criterion indicating that the flow in the vicinity of the model is that which the model would generate in an infinite flow field.

The location of the dividing streamline is now chosen as the location of one contoured flexible wall in a self-streamlining two-dimensional test section. The test procedure is to measure the pressures generated along the inside of the contoured wall, giving the real pressures distribution, P_r, calculate the boundary layer displacement thickness along the wall, determine the contour of the equivalent potential flow dividing streamline by adjusting the known wall contour by δ^*, utilize this dividing streamline contour as a boundary of the imaginary inviscid flow to calculate the imaginary pressure distribution P_i, and to maneuver the wall until the pressure distributions indicate zero imbalance along the length of wall. For the two-dimensional testing of a cambered airfoil, or a lifting symmetrical section, the procedure is necessarily carried out for one streamline above the airfoil and independently for one streamline below, since they will not have the same contours.

2.4 Ground-effect mode.

The flow to be generated in the self-streamlining wind tunnel is a portion of that about a pair of models, one being the mirror image of the other. The arrangement is illustrated on Fig. 1 (d). The test section bounds the real flowfield and contains one of the models. One wall represents the straight line of symmetry between the real and imaginary models, the other may follow any convenient streamline along the other side of the real model clear of its boundary layer.

Since one wall remains straight even though the pressure along it is non-uniform, the pressure being matched by an identical distribution from the image, it is necessary to apply the infinite field streamline criterion outlined above only to the contoured wall. The method may have application to testing in ground-effect, where a flat moving ground could replace the test section wall on the plane of symmetry.

2.5. Cascade mode.

Illustrated on Fig. 1 (e) is a portion of a cascade of cambered airfoils, one of which is real and mounted in the test section. The flexible walls are

shown aligned with streamlines passing between the airfoils, the walls having the same shape as each other and following identical streamlines spaced one foil-pitch apart. Since events along line A B C are matched by events along line A'B'C', a simple streamline criterion for cascade flow is that the pressure distributions along the walls should be equal when the walls are spaced one foil-pitch apart measured parallel to the leading edges. For example, the static pressure measured at wall station B should equal that vertically below it at B'. The cascade leading edge line L E is vertical. The flexible walls would be maneuvered with constant vertical spacing while achieving this equality in pressures.

Turbine and compressor cascades may be simulated, characterised by different values of a matching angle λ. This is the angle between the plane of the leading edges of the cascade and a normal to the incident airflow. The cascade streamline criterion requires the matching of test section wall pressures at points opposite each other on diagonals inclined at the matching angle. The cascade geometry is defined on Fig. 3 where an airfoil is illustrated having a circular-arc camber line of camber angle ω. The simulation is of turbine flow (an accelerating, or nozzle flow) or compressor flow (a decelerating, or diffuser flow) depending on whether $\lambda < \omega/2$ or $\lambda > \omega/2$ respectively. The special case of $\lambda = \omega/2$ involves flow turning without velocity change and represents, for example, a zero-reaction turbine rotor row, the impulse turbine.

Sketches of test section arrangements for these three cases are shown on Fig. 4. Note that the same airfoil and the same angle of attack are sketched as shown on Fig. 3 but to a different scale. The change from turbine flow, Fig. 4(a), to compressor flow, Fig. 4 (c), is achieved merely by changing the wall geometry. Lines AA', BB', CC' linking the flexible walls are sketched in the three illustrations, in each case parallel to the cascade leading edges. The separation of the walls measured along these lines would be held constant during the period when the walls were being manoeuvred to streamline contours. With subsonic flow through a cascade it would be necessary to make provision for contouring the test section some distance upstream and downstream of the airfoil, as suggested in Fig. 4 (b). In the case of a non-lifting uncambered model, the cascade and closed test section modes are identical.

3. Two-Dimensional Test Section Design.

3.1. Aerodynamic considerations.

Since the design of the test section being postulated is unconventional in respect to one important dimension, namely the height, it is necessary to consider all implications of the change, favourable or otherwise. A notional test-section design concept is developed at this point in order to illustrate the possibilities as seen at this stage. It should be emphasised that in many cases hard data cannot be offered to aid design decision making, because the research program is relatively new. In the actual design of the first test section, detailed in section 3.3, many decisions were based on engineering judgement.

The major advantages of the self-streamlining test section concept will be obtained when these test sections are designed to have their walls close to the model. The question arises as to how closely the model may be approached by the walls without interference. Of the many factors which could conceivably limit the closeness, one is fundamental, namely an incipient merging of the wall with the wake of the model. Most of the wall contour criteria described in the preceeding section rely on the flow just outside of the wall boundary layer remaining potential, the methods rely on the existence of constant stagnation pressure along the test section at the wall boundary layer edge. More specifically, the wall and model boundary layers must not merge. If the analogy is made with the entrance region of a pipe, then the test section must lie in the "entrance region" where a potential core exists. However, it is just conceivable that the boundary layers could be allowed to converge at the downstream end of the model, with some modification to the "streamline criteria" for the portion of the test section further downstream possibly involving the measurement of stagnation pressures in the manner of a wake traverse. The arrangement of model and test section which has now been arrived at is illustrated in Fig. 5 (a), which again shows a two-dimensional airfoil test. The shallow depth of test section confers on it a very unconventional appearance, long and narrow. It is conceivable that provided

the proximity of the wall to the model is acceptable, the length of test section normally considered necessary upstream and downstream of the model could be reduced. Such a test section is shown in Fig. 5 (b), its depth chosen by considerations such as discussed above. In this sketch the streamwise truncation is to regions where the flow is strongly deflected from the free-stream direction by the presence of the model.

The flow over the wing can now be considered originating in a jet, directed at the correct upwash angle, and contained in a correctly contoured glove. The test section contains a volume of air just sufficient to permit the correct modelling of that portion of the flowfield directly influenced by viscous action, the behavior of which is not considered amenable to analysis with certainty.

With this test section not only would there need to be provision for contouring the walls, but also provision for contouring portions of the contraction and first diffuser, since the majority of the tunnel circuit would be fixed in geometry. The contouring of these components would be required in order to provide the correct upwash and downwash angles. On Fig. 6 is shown a possible layout of the test section region of such a self-streamlining wind tunnel. For the accurate contouring of the walls a multiple jack system is required (a few are suggested in this figure along the upper wall). Furthermore, to hold the wing near the center of a narrow test section, there would be provision for translating the model vertically with change of angle of attack.

The effect of reducing the size of the test section on tunnel drive power may be derived if test conditions of Mach and Reynolds numbers, pressure, temperature and hence wing chord are assumed constant. Drive power ratio p, defined as the ratio of drive power for the self streamlining wind tunnel to that required in a normal tunnel, for a fixed aspect ratio of the wing is simply proportional to the depth ratio d. Depth ratio is defined as the ratio of the depth of the self-streamlining test section to a normal test section. Drive power is assumed proportional to flow area.

A case can be seen for possibly reducing aspect ratio with depth ratio. When the depth becomes very small the pair of flow channels

at the model, one over and one under the wing, become slit-like viewed along the stream. It is possible that the flow would also become highly two-dimensional, with the secondary flow disturbances receding toward the side-walls. Therefore the aspect ratio might be reduced without degradation of data quality. If a is defined as the ratio of the wing aspect ratio employed in the self streamlining tunnel to that used in conventional tunnels, then tunnel drive power ratio may be written:

$$p = ad$$

Drive power ratio is plotted on Fig. 7. Conventional tunnels have $p = a = d = 1.0$. The test section described later has depth and power ratios of approximately 0.28, with conventional values of aspect ratio being used. The point is shown on Fig. 7. However, the advantages in terms of energy demand of reducing both aspect ratio and depth are apparent from the figure, and development effort in the general direction indicated on the figure would be rewarding.

Very approximate limits on depth ratio may be derived from the application of flat-plate turbulent boundary layer theory to the wall and model. The model is assumed to be placed at the center of the test section. The length of test section from its entrance to the wing trailing edge is ℓ wing chords, and the variation of boundary layer thickness δ is given by

$$\frac{\delta}{x} = \frac{k}{R_x^{\,m}}$$

where x is measured from the leading edge of the wing or test section as appropriate, and k and m are constants.

It can be shown that the ratio of test section depth to wing chord, with boundary layers merging at the trailing edges is given by

$$2k(1 + \ell^{1-m})/R_c^{\,m}$$

For the case of $\ell = 5$, with the commonly adopted values $k = 0.376$ and $m = 1/5$, depth ratios d of 0.0548 and 0.0218 result at chord Reynolds numbers of 10^6 and 10^8 respectively. A ratio of test section depth to wing chord of 4 was assumed for conventional two dimensional tunnels.

These limits are shown on Fig. 7. It can be seen that relatively large reductions in drive power requirements would result from the use of test section configurations close to such limits.

3.1.2. The first series of tests contemplated for this flexible walled test section were on a circular cylinder mounted normal to the flow. It was decided not to attempt at this early stage the type of construction shown on Fig. 6, but to extend the test section sufficiently far up-stream for the flow at entry to be considered undisturbed to any significant extent by the model. In subsonic flow the model disturbs air infinitely far upstream, and therefore the choice of the extent of its influence is arbitrary, depending on the interpretation of the word "significant".

There is no advantage in extending the flexible walls upstream beyond the point where the free stream has been deflected from its undisturbed path by an amount equal to the mechanical resolution expected in setting the walls, or beyond the point where the pressure disturbance due to the presence of the model is equal to pressure resolution. Incompressible potential flow theory was used as a guide in the determination of these points, the position of which could determine the point where the flexible wall is fixed, the wall origin or anchor point. The results of the computations are presented in non-dimensional form on Fig. 8 which shows part of the upper half of the infinite flowfield approaching a cylinder. The non-dimensional deflection ε of a streamline from its undisturbed path is defined as $\varepsilon = \delta/r$ where δ is the deflection of the streamline caused by the cylinder, and r is the radius of the cylinder. ε is constant along circles centered on the Y-axis. Segments of the circles are shown as broken lines on Fig. 8. Practical constraints on test section width suggested the use of a cylinder of radius not greater than one inch. The resolution in the measurement of wall position was expected to be two or three orders of magnitude smaller, hence ε would have

a low value in the range 0.001 to 0.01. At a given streamwise distance from the model, low values of ϵ are obtained both close to and far from the X-axis which is a line of symmetry on Fig. 8. At a given distance from the X-axis ϵ falls with increasing distance from the model.

If position resolution is assumed independent of test section size, then for a given cylinder ϵ is constant and as suggested earlier might lie in the range 0.01 to 0.001 for the present model. Fig. 8 shows that for example if $\epsilon = 0.005$ is chosen, a streamline passing through $Y = y/r = 10$ is deflected by this amount relatively far upstream at a station 43.7 cylinder radii ahead of the model, whereas a streamline closer to the X-axis, say passing through $Y = 1$, suffers the same deflection much closer to the model, at $X = 15$. Therefore, for a cylindrical model, consideration of wall position resolution suggests that a shallow test section be used, because it can also be short.

Consideration of pressure resolution provides another fix on test section length. It is easily shown that for two-dimensional incompressible potential flow around a cylinder the pressure in the flow field is given by $C_p = \frac{2(X^2 - Y^2) - 1}{(X^2 + Y^2)^2}$, where X and Y are the axes of Fig. 8. Contours of constant C_p are shown. In 90° sectors above and below the model, C_p is negative. C_p is zero along the curves $X^2 = Y^2 + 1/2$ which asymtote to 45° slopes, while upstream of the model C_p is positive. With the combination of dynamic pressure to be used in these tests (equivalent to 3 or 4 inches of water) and pressure resolution (about $\pm$ 0.02 inches), values of C_p less than about $\pm$0.006 could not be resolved. Therefore on this basis there was no point in extending the flexible walls upstream to regions where lower values of C_p would be expected.

The beginning of the flexible portion of the test section which has been chosen is indicated on Fig. 8. At this point, according to the above theories, the cylinder would produce a pressure coefficient of 0.0033 and a streamline dimensionless displacement $\epsilon = 0.0058$. The test cylinder had a radius of 0.875", and therefore at the wall origin the streamline which is to be represented by the wall would have been displaced from its position in undisturbed flow approximately 0.005 inches, a distance which can just be

resolved by the equipment in use.

One further important aerodynamic limitation on wall proximity could be set by a separation of the wall boundary layer. In the limit as the wall is brought closer to the model, the wall carries the same pressure distribution as the model. Since the boundary layer on the wall is thicker than on the model it would separate first. Such a separation is undesirable on account of the unsteadiness so introduced, and because the various streamline criteria outlined in section 2 rely on the flow near the walls following the wall contours. It would be difficult to make proper allowance for the distribution of boundary layer displacement thickness in the presence of separation.

3.2. Mechanical considerations.

3.2.1. Wall thickness and loading.

A compromise had to be sought between conflicting requirements. For the generation of a particular streamline contour, a thin wall would experience the lowest stresses and be least demanding on jack forces, but would also be least resistant to inter-jack deformation from streamwise compressive or tensile loads or from any pressure differences across the wall.

The actual design of test section minimised this pressure difference by providing outside of each wall a plenum chamber communicating with the test section well downstream of the model. The tunnel is atmospheric and therefore the peak pressure difference was thereby reduced from around 1 1/3q to 1/3 q.

Acrylic plastic had been chosen as the wall material with a thickness of one-sixteenth of an inch. Since pressure difference and streamline curvature were both likely to peak near the model, the jacks were pitched more closely here than elsewhere. This wall material has low strength, and the bending stresses were checked using the potential flow around a cylinder as a guide to streamline curvature.

Along a wall following a streamline toward this model there are two minimum radii of curvature, and therefore two stress peaks. The first occurs ahead of the model where the inside of the wall is under tension,

the second inline with the axis of the model where the outside of the wall is in tension. For all streamlines except those passing close to the model (that is, for all streamlines except those which spring from a height above or below the axis equal to or less than 0.311r infinitely far upstream) the higher of these stresses occurs alongside the model. The streamline which passes through the point identified on Fig. 8 as the upstream end of the flexible wall experiences a first peak stress of approximately 155 psi at a point 3.8 r upstream of the cylinder, and a second peak of 555 psi inline with the model. The latter figure is about one tenth of the 1000-hour fracture stress for this material, which leaves an adequate allowance for stress raisers.

3.2.2. Automatic control.

The present test section is manually adjusted. However, it is highly desirable that any future design should have provision for the automatic control of the walls. This feature should be relatively easily incorporated by scanning the wall pressure and position distributions, with on-line computation and feedback of wall adjustments, and with certain safeguards to protect the walls from overstressing during normal operation or following malfunction of the controls. This suggested pattern of events is identical to that followed in a manual mode with the present tunnel.

3.3. Test-section design.

An atmospheric, open-return low speed fan driven wind tunnel having a 12 inch square test section was available for modification. The combination of the speed capability of the tunnel with a desire to test at the upper end of the subcritical Reynolds number range for cylinders (around 10^5 based on diameter) led to the choice of the 1.75-inch diameter cylinder. Following the reasoning outlined in the preceeding sections, a pair of flexible walls was incorporated inside the existing test

section, reducing its depth to a nominal 6 inches, while retaining the full width of 12 inches. Models of 12 inch span can be mounted horizontally mid-way between the flexible walls. The length of flexible wall upstream of the cylinder axis is 21 inches. At this distance upstream, relative to free stream values both the streamlined wall pressure and its displacement are close to the limits of resolution. The upstream ends of the flexible walls were fixed in position, and the tunnel contraction was modified to suit the new test section proportions. The flexible walls extend downstream of the cylinder center-line an arbitrarily chosen distance the same as upstream, 21 inches, making a total test section length of 42 inches, 24 cylinder diameters. On each wall are arranged transversely 15 stiffening ribs, at each of which is a pressure orifice for measuring the "real" static pressure at the wall. The wall position is adjusted by screw-jacks attached to each rib. A cross section of the test area is shown on Fig. 9. Measured from the wall anchor points the ribs are located nominally at stations 6, 9 1/2, 12 1/2, 15 1/2, 17 1/2, 18 1/2, 19 1/2, 20 1/2, 21 1/2, 22 1/2, 23 1/2, 24 1/2, 26 1/2, 29 1/2 and 33 1/2 inches downstream. The jet emerging from the test section is discharged directly into the unmodified original diffuser.

Details of the rib, orifice and jack design are given on Fig. 10. To accommodate varying slopes of the walls, flexures were chosen in preference to pivots in order to eliminate free motion which could have been a source of vibration near lightly loaded jacking points. The short length of the flexures allows them to carry adequate compressive loads without buckling.

The long edges of the flexible walls clear the solid sidewalls by approximately 0.03 inches to allow free movement. The gap is closed with a rubber seal bonded to the flexible wall, a feathered edge on the seal touching the sidewall.

There is a relatively long section of flexible wall downstream of the last jack. Originally the wall terminated just 2 inches downstream of that jack. However, it was found that the pressures recorded at the downstream orifices were not consistent with expectations because they were being influenced by the static pressure in the plenum chambers outside of the flexible walls. Therefore, the walls were extended in straight lines downstream by 6.5 inches in order to reduce the coupling between the plenum and test section. In its present form the test section is performing satisfactorily.

Two measurements are made at the walls during test runs, namely pressure and position. Pressures are measured on alcohol manometers, giving a resolution in terms of pressure coefficient of about ± 0.006. Wall position is measured with a dial gage to an accuracy estimated to be in the range ± 0.003 to ± 0.005 inches. In terms of test section half-height the larger figure is ± 0.00167, and in terms of test cylinder radius ± 0.00571.

4. Computation of the Imaginary Flowfields.

4.1. Wall boundary layer corrections.

The equivalent top and bottom wall contours felt by the potential flow around a two-dimensional model are the actual wall contours corrected for the distribution of the boundary layer displacement thickness δ^*. In practice the walls are adjusted for constant static pressures in the absence of the model at a standardised unit Reynolds number. Since the side-walls are parallel, the flexible walls accommodate all of the empty test-section boundary layer growth. The flexible walls diverge in the streamwise direction but are subject to uniform pressure and velocity, and are therefore assumed to develop a turbulent boundary layer according to the conventional flat-plate empirical relationship

$$\frac{\delta^*}{x} = \frac{0.0322}{R_x^{1/6}} \qquad \text{4.1.}$$

In this equation x is the distance downstream from the origin of the flat plate which is taken to be the downstream end of the contraction, and R_x is the Reynolds number based on x. The normal value of the unit Reynolds number was 0.68×10^6 per foot.

In the presence of a model all four walls are subject to different pressure and velocity fields. The sidewalls experience the strongest pressure gradients and resultant disturbances which can include separation, and consequently the largest local changes of boundary layer displacement thickness. However, on this model the only measurements which were to be made were of pressure around the center-span, a position relatively remote from the side-walls. The measuring station was in much closer proximity to the flexible top and bottom walls than the sidewalls, the distance to the sidewalls being 2.8 times the distance to the flexible walls. Therefore, pressures on the model at the measuring station are likely to be most strongly affected by changes in δ^* on the flexible walls. The variation of δ^* in the presence of the pressure gradient along the flexible walls walls was computed from the Von Karman momentum integral equation

$$\frac{d\theta}{dx} + 3.4 \frac{\theta}{u} \frac{du}{dx} = \frac{0.0128}{R_\theta^{1/4}} \qquad \text{4.2}$$

where θ is the boundary layer momentum thickness, assumed here to be $\delta^*/1.4$, u is the local velocity outside of the boundary layer, and R_θ is a Reynolds number based on θ and u. The equation was solved numerically using the measured distribution of velocity along the wall centerline. Examples of predictions of the programme are given on Fig. 11. A satisfactory prediction of δ^* is demonstrated for the case of zero pressure gradient.

By setting the walls to constant pressures an allowance is automatically made for the development of δ^* through the empty test section. This wall setting is taken as being "straight". In the general case with a contoured wall and a model present, the changes in δ^* due to pressure gradients are used as corrections to the geometrical profile, giving an "effective" wall contour, the contour which ultimately must become a streamline. For example, if at one station along the wall during the process of moving towards the shape of a streamline, the wall has been moved away from the model a distance y, but at this same station due to the finite pressure gradients which then exist the boundary layer displacement thickness is less than the empty test section value by $\Delta\delta^*$, the "effective" movement of the wall away from the model is $y' = y - \Delta\delta^*$. In the example shown on Fig. 11, $\Delta\delta^*$ peaks adjacent to the model with a value of about -0.018 inches. The imaginary part of the flowfield is computed flowing over the outside of the effective contour.

4.2. The imaginary flowfield.

An analytical derivation of pressures generated at the walls by this flowfield is required in the streamlining procedures in the free flight and ground effect modes. In the two-dimensional free flight mode there are two imaginary fields separated by the real flowfield passing along the test section. The imaginary fields are treated analytically independently of each other, but have common values of free stream properties far upstream. In the ground effect mode of operation there is only one imaginary flowfield to compute since one wall has an effective contour which is a straight line. Note that in order to obtain an effectively straight wall, the wall has to be deflected by $\Delta\delta^*$.

Each imaginary flowfield extends in principle infinitely far away from the test section. In the ideal case the field is bounded on one side by a surface lying parallel to the free stream vector far upstream of the test section, the surface blending into the effective contour of

the flexible wall. The contour introduces a disturbance into the imaginary field.

The shape of the surface downstream of the test section depends upon the model and on the mode of operation of the test section, but in the modes considered here, free flight and ground effect, far downstream of the model the surface again tends towards the freestream direction.

The Mach number of these tests is about 0.1, and therefore an incompressible and also inviscid solution to the imaginary flowfield has been used, for the reasons outlined in section 2.3.

The method of computing the imaginary pressure coefficient distributions along the walls is under continuous development. At the present time, C_{p_i} is computed on a boundary to the imaginary flowfield having a shape which is approximately the same as the effective wall contour. The boundary is represented in the computations by the envelope of the flow from a finite number of finite strength sources and sinks. The sources for a wall are located midway between jacks, along a straight line, with one additional source located midway between the upstream anchor point of the wall and the first jack, making 15 sources in all for each wall.

An approximate estimate is first made of the strengths of the row of fifteen sources/sinks. In cases such as this, where the slope of a wall is small, it can be shown[6] that wher the wall is produced by continuously distributed source, the source has a strength s per unit length of test section given by

$$s = u \frac{dy'}{dx} \qquad \text{4.3}$$

where x has its origin at the wall anchor point and is measured downstream parallel to the free stream, y' is the effective displacement of the wall from straight, and u is the free stream velocity. The sources are assumed to discharge only to one side of the line containing them, that is on the imaginary flowfield side of the x-axis for that wall.

The slope dy'/dx mid-way between each jacking point was determined by curve-fitting the co-ordinates of the effective wall. The resultant value of s was taken to represent the average strength per unit length between the pair of jacks. A finite source having a strength equal to the product of s with the jack spacing was then assumed to lie midway between the jacks. Therefore, between any pair of jacks having co-ordinates x_{n-1} and x_n a source of strength

$$S_n = s_n (x_n - x_{n-1}) = u \left(\frac{dy'}{dx}\right)_n (x_n - x_{n-1}) \qquad \text{4.4}$$

was assumed to lie on the x-axis at position $1/2 (x_n + x_{n-1})$.

The position of the wall is known, within the resolution of position measurement, at 16 points. These are the 15 jack locations plus the anchor point. The 15 sources so determined lie-midway between each of these points.

The wall generated by this set of sources has been found to depart from the required shape by amounts well exceeding the resolution of position measurements. For example the y' - co-ordinate of one such wall differed from the value set by a maximum of 0.043 inches, whereas y-position resolution is about $\pm$ 0.003 inches. This maximum error occurred at a position along the test section close to the model where the value of y was 0.591 inches and the value of C_{pi} on this approximation to the required wall shape was -0.1.3. Since the resolution in C_{pr} is $\pm$0.006, there appeared to be room for improvement in computational technique judging from the discrepancy in shape revealed above. However, the computations were aimed at determining $C_{pi}(x)$ but not necessarily y'(x) within the limits of their respective real-side experimental resolutions.

A technique for adjusting the values of the source strengths has been developed which allows the matching of the resultant potential-flow

wall positions with y' at the jacking points, within any set limits. It should be noted that the location of the potential-flow wall at a particular jack is determined by integrating, between the x-axis and the wall, the flow which crosses a perpendicular to the x-axis at the jack. The flow is equated to the summation of the sources upstream of the jack. The computational technique adopted simply required the adjustment of the strength of the source immediately upstream of the jacking point being considered, until the position of the potential wall agreed with y' within limits. The limits adopted are $\pm$0.002 inches. On moving to the computation of the location of the wall at points downstream, the strength of the source so determined was held constant at the new value. Following adjustment to the strengths of all sources the cycle was repeated until no change in source strength was demanded. Four cycles are normally sufficient. The potential flow boundary shape then agreed to that required at the jacking stations to an accuracy of approximately $\pm$0.002 inches, which is just inside the resolution of position measurement.

In the preceding example, the resultant value of C_{pi} is -0.158, different by the significant amount 0.035 from that given by the first approximation. This is some justification for the adoption of the improved technique.

An example of a contour y'(x) and the variation of C_{pi} along it, computed according to the preceding methods, is shown on Fig. 12.

4.3 Experimental simulation of the imaginary flowfield.

It is possible to verify the theoretical predictions of the above section. The options available to reproduce the imaginary flowfield are the use of an electrolytic tank, or the use of a wind tunnel. In practice, only a limited portion of the infinite flowfield can be reproduced at any one time. It is necessary to include the wall contour as one boundary, with the other boundaries in the experimental reproduction of the flowfield positioned as far away as possible. In principle large areas of the flowfield could be reproduced section-by-

section in the experiment, with boundary conditions matched between adjacent sections.

It is difficult to reproduce compressibility effects in the electrolytic tank, otherwise it is an attractive option particularly to complement low speed wind tunnel tests. However, the wind tunnel method of reproducing the imaginary flowfield was adopted because ultimately this method would be superior for use in high speed testing, and it seemed desirable to gain some experience.

The method is summarised on Fig. 13. Following a test with the model present, the effective wall contours are known as sketched in Fig. 13(a). The imaginary flowfields above and below the effective wall contours are computed. One is sketched in Fig. 13 (b). The pressure distribution C_{pi} is derived from the computations, and also the shape of a streamline one test-section-depth away from the wall, inside the imaginary flowfield. This portion of the imaginary flowfield is simulated in the wind tunnel, a portion equal in depth to the test section depth. The test arrangement is shown on Fig. 13 (c), allowing C_{pi} to be measured.

The measured and computed values for C_{pi} are shown in Fig. 13(d), for the wall contour shown on Fig. 12. The locations of the peak positive and negative pressures given by the two methods are in good agreement. The peak pressure coefficients differ by 0.025 and 0.01 respectively, only just outside the limits of pressure resolution. The values of C_{pi} predicted by theory are therefore considered adequate for the present purposes.

5. Convergence of Wall Contours to Streamlines.

5.1. The mismatch elimination procedure.

The combined information comprising the wall position and real side pressure coefficient distribution $C_{pr}(x)$ and the free stream conditions, allows the computation of a pressure imbalance distribution $C_{pi} - C_{pr}$ along the wall. Various methods for eliminating the error have

been tried; none is regarded as ideal. The simplest method and as yet one of the most effective has been to move the wall locally for the next run away from the X-axis a distance Δy proportional to the local pressure imbalance $C_{pi}-C_{pr}$ across the wall streamline. A displacement coefficient ϕ, defined by $\phi = \frac{\Delta y}{(C_{pi}-C_{pr})} \cdot \frac{1}{\text{test section depth}}$ is a convenient constant of proportionality.

In most of the testing carried out so far, ϕ has been given the value 0.06. With this value, convergence of the wall shape to the required streamline shape has been relatively stable and monotonic. Lower values simply prolong the iteration process, but experience has shown that values much higher, say greater than about 0.1, result in an oscillatory nature of wall shape between one setting and the next, combined with high local stresses. The high stresses and oscillations in demanded wall position occur in the portions of test section adjacent to the model, and are absent upstream and downstream. They appear to be a limiting factor in the rate of convergence of the walls to streamlines with this iterative method. No doubt other methods can be devised exhibiting more rapid convergence combined with the damping necessary to prevent position oscillations and over-stressing.

In judging the acceptability of a particular wall contour, a measure of the mismatch in pressure coefficient between the real and imaginary flows either side of a wall may be used as a guide. The measure adopted is the average in $|C_{pi} - C_{pr}|$ for the 15 locations along the wall. It is feasible with the present equipment to obtain values of this average between 0.01 and 0.02.

5.2. Examples of the iteration process.

These examples apply to tests on the circular cylinder. Fig. 14 shows E the value of the average of $|C_{pi} - C_{pr}|$ at each of the iteration steps in moving from the cascade-mode straight wall configuration toward the infinite flowfield mode. The value of ϕ has been held constant at

0.06 in these tests. An approximate number of iterative steps of 8 is indicated by this data in order to move from the straight wall configuration to the infinite flowfield configuration giving a value of E of less than 0.02.

In one typical test series, not that shown on figure 14, where the iterations were terminated when E reached 0.01, the maximum local value of the pressure imbalance $|C_{p_i} - C_{p_r}|$ was 0.033, while the arithmetic mean imbalance was 0.003.

6. Aerodynamic Data.

6.1. Pressure distributions around a cylinder.

A standard test velocity was chosen such that the Reynolds number obtained was near the upper end of the subcritical range with the 1.75 inch diameter cylinder. The test Mach number was approximately 0.1, and the Reynolds number based on diameter was approximately 10^5. The model had a smooth surface, and was fitted with a single pressure orifice mid-way along its span allowing pressure distributions to be obtained by rotating the cylinder about its axis. The same orifice measured tunnel stagnation pressure which was used in conjunction with a reference static pressure in determining free stream dynamic pressure.

6.1.1. Infinite flowfield mode.

The test section top and bottom walls were gradually formed into the shapes of streamlines in an infinite flowfield during this series of tests. Each wall was treated independently, and at each step in the iterative procedure measurements were made of the wall contours and static pressure distributions. From the imbalances in pressure revealed by computations of the imaginary flowfields outside of the top and bottom walls, each was moved locally a distance proportional to the local imbalance. This procedure was terminated when the measure of average

imbalance E appeared to have reached a minimum. The pressure distribution around the model was then taken.

On Fig. 15 the distribution is compared with the data of Fage and Falkner[4] taken under lower blockage conditions. The Reynolds numbers were very close. A value of 1.06×10^5 is quoted in reference 4, while the data taken in the flexible wall test section was at 1.03×10^5.

Sets of curves on Fig. 15 show pressure distributions at three values of tunnel blockage, defined as the ratio of cylinder diameter to tunnel depth. The 6.1% and 12.3% blockage data is taken from reference 4 where the cylinder diameters were 2.93 inches and 5.89 inches respectively, tested in a 4 foot deep test section. The 29.3% blockage data was obtained in the 6 inch deep flexible walled test section on the 1.75 inch diameter cylinder. Three curves show the measured pressure distributions in the presence of straight walls. The 6.1% and 12.3% blockage data is also shown corrected for wall interference, by the methods of Allen and Vincenti[5], to give the infinite-flowfield pressure distributions. Also shown is the uncorrected pressure distribution taken in the Self Streamlining Wind Tunnel with the walls streamlined for an infinite flowfield. There is good agreement between the latter three sets of points.

Comparisons may also be made between drag coefficients obtained from pressure distributions. The average value for the drag coefficients of the two cylinders from reference 4, corrected for wall interference by the methods of reference 5, is 1.129. A drag coefficient of 1.136 was obtained in the flexible walled test section. These coefficients agree to within 0.6%.

The close agreement revealed by this data is the basis for a claim that the Self Streamlining Wind Tunnel is capable of producing interference-free flow conditions around a model even in high blockage situations.

6.1.2. Cascade and open-jet modes.

It is often supposed that a two-dimensional test on a model such as a cylinder in a closed test section generates flow around the model as though it was one of an infinite cascade of models. The models in the cascade are pitched evenly apart a distance equal to one test-section depth, if the model is mounted in the center of the test section. This supposition is not strictly true, even for the case where the span of the model is very large such that end-effects can be ignored. The reason is that the boundary layer along the top and bottom walls distorts in thickness due to the pressure field generated by the model. In the case of a cylindrical model, where low pressures exist at the walls adjacent to the model, the boundary layer displacement thickness is reduced in comparison with the value obtained at the same Reynolds number in the empty test section. To simulate cascade flow the walls must be moved towards the model to compensate. In low-blockage tests the effect may be small, but in this flexible walled test section the effect in terms of pressure distribution around the cylinder is measurable. Data taken with the walls straight, and with them curved to generate cascade flow, is shown on Fig. 16. Significant differences in pressure coefficient exist, amounting to about 0.05 around the rear half of the cylinder, and between 0 and 0.1 over the front half.

Shown also on Fig. 16 is the pressure distribution in the open-jet mode, taken with the walls set for constant static pressure equal to tunnel reference static pressure. The infinite-flowfield data is repeated for comparison. Evidently with high blockage an open jet test could be expected to give data closer to that obtained in an infinite flowfield than would a closed test section. No comparative open-jet data has been found in the literature.

6.1.3 Ground-effect mode.

The cylinder was tested in ground effect by setting one wall to

represent flat ground and the other to follow a streamline in an infinite flowfield above the cylinder. Checks were made in this and other tests that the top and bottom wall boundary layers did not separate.

With the model in the center of the test section a height between ground and cylinder axis of 1.71 diameters was simulated. The test data is shown on Fig. 17, where the main differences in pressure are seen to occur over the leading half of the cylinder. The stagnation point has moved only about 2 degrees from the leading edge of the cylinder towards the ground, producing a small lift effect and a lift-drag ratio of 0.038.

6.2. Wall Contours.

The contours of the flexible walls adopted during the various modes of operation are illustrated in sketch form on Fig. 18. The distortion in boundary layer thickness between (a) and (b) illustrates the need to move the walls locally towards the model to simulate the cascade flow in (c). Again, there are significant changes in δ^* in the infinite flowfield mode (d) which must be taken into account. Only in the open-jet mode (e) is there no change in δ^* between a test with the model present and the walls contoured, and with an empty test section and the walls "straight". The ground-effect mode (f) requires one wall to be curved to produce a straight δ^* line, which becomes the effective position of the ground, and one wall to be curved in order to match the real and imaginary flowfields.

Plots of the wall contours set during these tests are shown on Fig. 19. In the cases of the open-jet, infinite flowfield and cascade modes, since the model was non-lifting the contours adopted by the walls were symmetrical. Therefore, each single curve describes the shape of the pair of walls.

In the ground-effect mode, the ground wall required to be deflected only a small amount, comparable to the cascade contour shown on Fig. 19. All of the wake thickness was accommodated by the other wall

which required a deflection of about one inch. In contrast the combined deflection of both walls in the open-jet and infinite flowfield modes amounted to a little over one inch.

Despite the fact that the test section is long, in some cases the walls do not tend toward zero slope at the upstream end of the test section. This indicates that the flow is being disturbed by the cylinder to a significant extent even twelve diameters upstream of its axis. Therefore the test section does not contain undisturbed flow anywhere, making the validity of the dynamic pressure in such a test questionable when estimated from pitot and wall static pressure measurements.

7. Discussion.

The techniques outlined in this Report are believed to have been satisfactorily tested and are in the process of achieving the objects of the research. However, several questions are raised which may not be rapidly answered without further determined effort, and a case exists for setting in motion the necessary experimental and theoretical research. The more important areas include -

(i) the determination of permissible wall closeness to the model,

(ii) the variation in the required aspect ratio of a two-dimensional wing, tested with top and bottom walls close to the wing,

(iii) the determination of the required length of test section, or the development of techniques allowing the use of short test sections having nowhere upstream any flow which can be considered close to free stream,

(iv) the development of techniques for attenuating shock reflections from non-porous walls,

(v) a study of mechanical configurations of three-dimensional flexible walled test sections, possibly for use in the low speed, high angle-of-attack testing of aircraft models.

Favourable outcomes from such research could be most rewarding in terms of the quality and cost of future aerodynamic testing. When combined with current developments in the art of wind tunnel testing, the total effect could be the realization of the long sought but elusive goal of test conditions truly representative of flight.

8. Conclusions.

(i) The achievement of interference-free flow around a bluff two-dimensional body has been demonstrated under high blockage conditions in a low speed wind tunnel fitted with self-streamlining flexible walls.

(ii) Techniques have been developed and utilised to satisfactorily converge the flexible walls to the contours of streamlines in an infinite flowfield.

(iii) Five significant modes of operation of a self streamlining wind tunnel have been identified, the test section being capable of simulating testing in: -

a conventional closed test section,
an open-jet
an infinite flowfield
ground effect
cascade

(iv) Criteria for ensuring the correctness of wall contours have been established and employed for each of the above modes of operation.

(v) In setting the above modes of operation, including the infinite flow-field mode, the measurements required in a flexible walled test section are of wall static pressure and wall position. These are both particularly simple measurements to make with adequate resolution, in contrast with the measurements of flow angularity and static

pressure in the stream which are required when infinite flowfield conditions are created in a straight, porous walled test section.

(vi) The demonstration of interference free flow with a high blockage model raises the possibility of increasing test Reynolds numbers in two-dimensional testing.

(vii) This work has pointed the way toward the possible elimination of the need for a plenum chamber with ventilated walls. Advantages would include a reduction in flow turbulence, and in transonic testing a reduction in tunnel drive power.

(viii) Testing in flexible walled test sections requires extension to higher Mach numbers, and to lifting wings, in order to further demonstrate the streamlining criteria.

(ix) Limits need to be established on the permissible closeness of the walls to the model, and on the length of test section necessary up- and down-stream of the model.

(x) The rate of convergence of the walls to streamlines is too slow using present methods. It would be an advantage to devise more rapid methods.

9. References.

1. Lock, C. N. H., and Beavan, J. A.: Tunnel Interference at Compressibility Speeds using the Flexible Walls of the Rectangular High Speed Tunnel. British ARC R. & M. 2005, 1944.

2. Ferri, A., and Baronti, P.: A Method for Transonic Wind-Tunnel Corrections. AIAA Journal Vol. 11, No. 1, Jan. 1973, pp. 63-66.

3. Sears, W. R.: Self Correcting Wind Tunnels. The Sixteenth Lanchester Memorial Lecture of the Royal Aeronautical Society, London, May 1973, and the Aeronautical Journal, Feb. 1974, 80-89.

4. Fage, A., and Falkner, V. M.: Further Experiments on the Flow around a Circular Cylinder. British ARC R. & M. 1369, 1931.

5. Allen, H. J., and Vincenti, W. G.: Wall Interference in a Two-Dimensional-Flow Wind Tunnel, with Consideration of the Effect of Compressibility. NACA Report 782.

6. Duncan, W. J. Thom, A. S., and Young, A. D.: Mechanics of Fluids, Arnold, 1970.

10. Symbols.

a	ratio of aspect ratios
c	wing chord
C_p	pressure coefficient
C_{pi}	pressure coefficient at the wall on the imaginary side
C_{pr}	pressure coefficient at the wall on the real side
d	cylinder diameter, or test section depth ratio
E	mean modulus of pressure coefficient imbalance along wall
k	a constant
l	test section length upstream of wing trailing edge in chord lengths
m	a constant
p	drive power ratio
P_i	static pressure on the imaginary side of the wall
P_r	static pressure on the real side of a wall or streamline
q	dynamic pressure $1/2\ \rho_\infty V^2_\infty$
r	cylinder radius
R	Reynolds number
s	local source strength per unit length of wall
S	strength of a finite source mid-way between jacks

u	velocity just outside the boundary layer
v_∞	free stream velocity
x	distance from boundary layer origin, or distance upstream of cylinder axis
X	dimensionless distance x/r upstream of cylinder axis
y	total movement of wall away from model, from its straight setting, or distance above cylinder axis
y'	effective movement of wall
y_∞	height of a streamline above the x-axis in undisturbed flow
Δy	movement required of wall away from the model, suggested by imbalance $C_{pi} - C_{pr}$
Y	dimensionless distance y/r above cylinder axis
δ	boundary layer thickness, or deflection of streamline
δ^*	displacement thickness
ε	δ/r, the dimensionless deflection of a streamline
θ	momentum thickness
λ	sweepback angle of the leading edge plane of a cascade
ρ_∞	free stream air density
ϕ	displacement coefficient
ω	blade camber angle

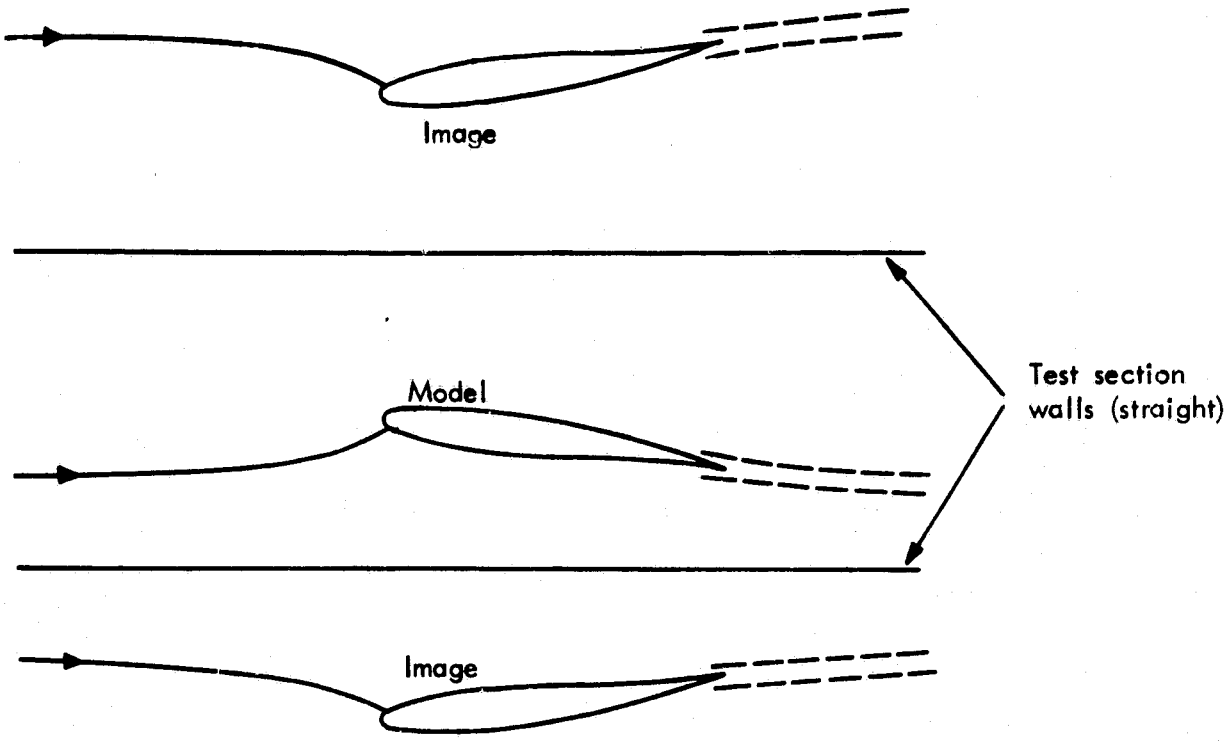

(a) Conventional closed test section mode.

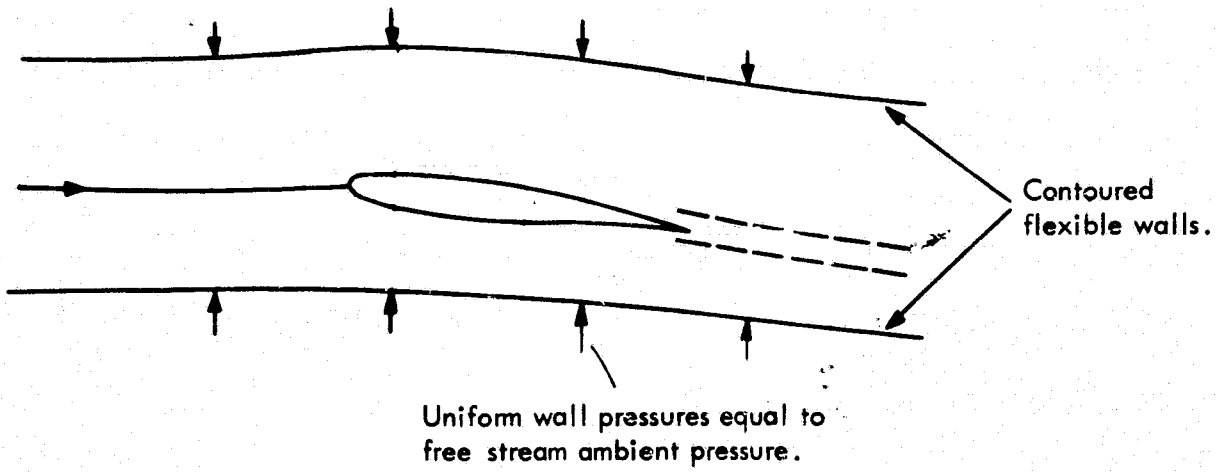

(b) Open-jet test section mode.

FIG. 1. ILLUSTRATIONS OF FIVE OPERATIONAL MODES OF THE SELF STREAMLINING WIND TUNNEL.

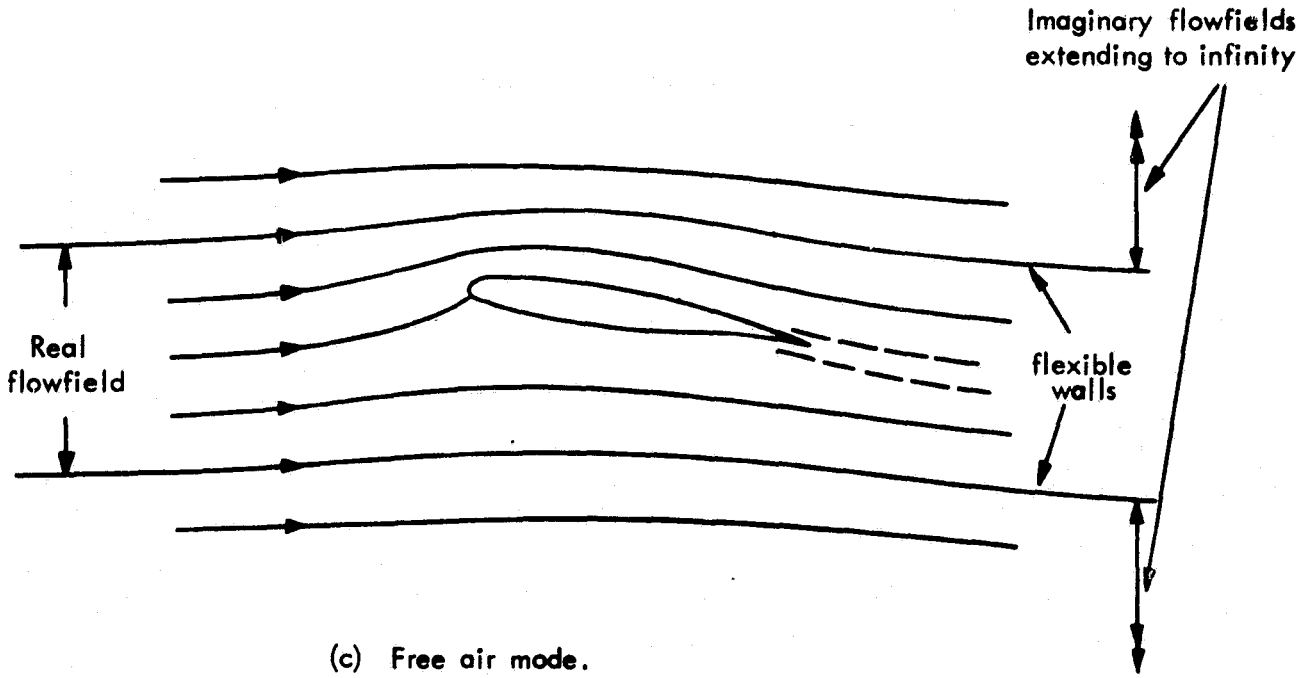

(c) Free air mode.

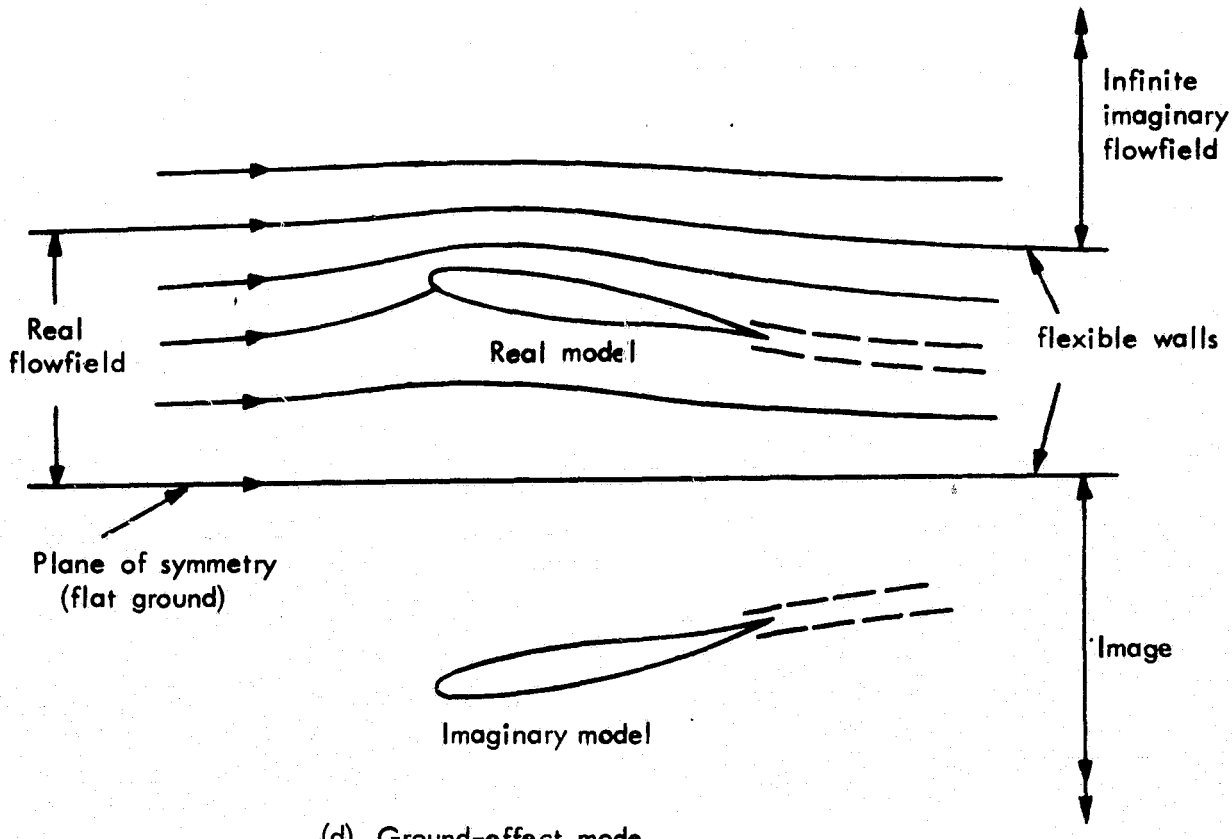

(d) Ground-effect mode.

FIG.1. ILLUSTATIONS OF FIVE OPERATIONAL MODES OF THE SELF STREAMLINING WIND TUNNEL (CONTINUED.)

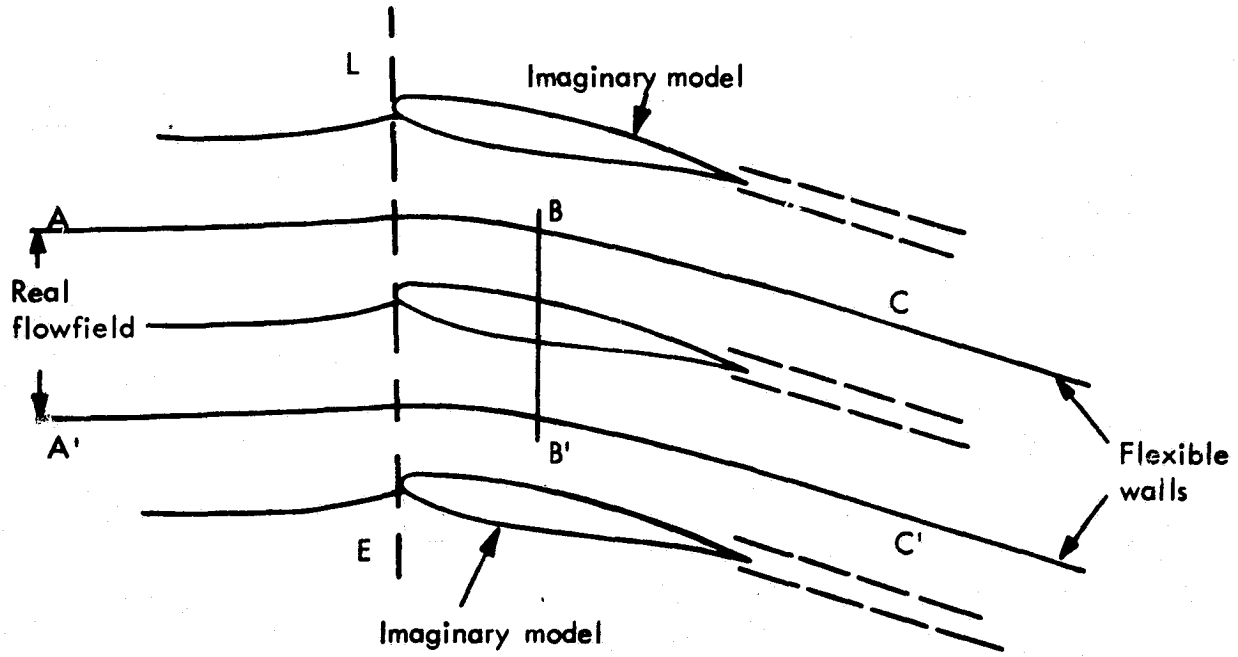

(e) Cascade mode.

FIG.1. ILLUSTRATIONS OF FIVE OPERATIONAL MODES OF THE SELF STREAMLINING WIND TUNNEL (CONCLUDED.)

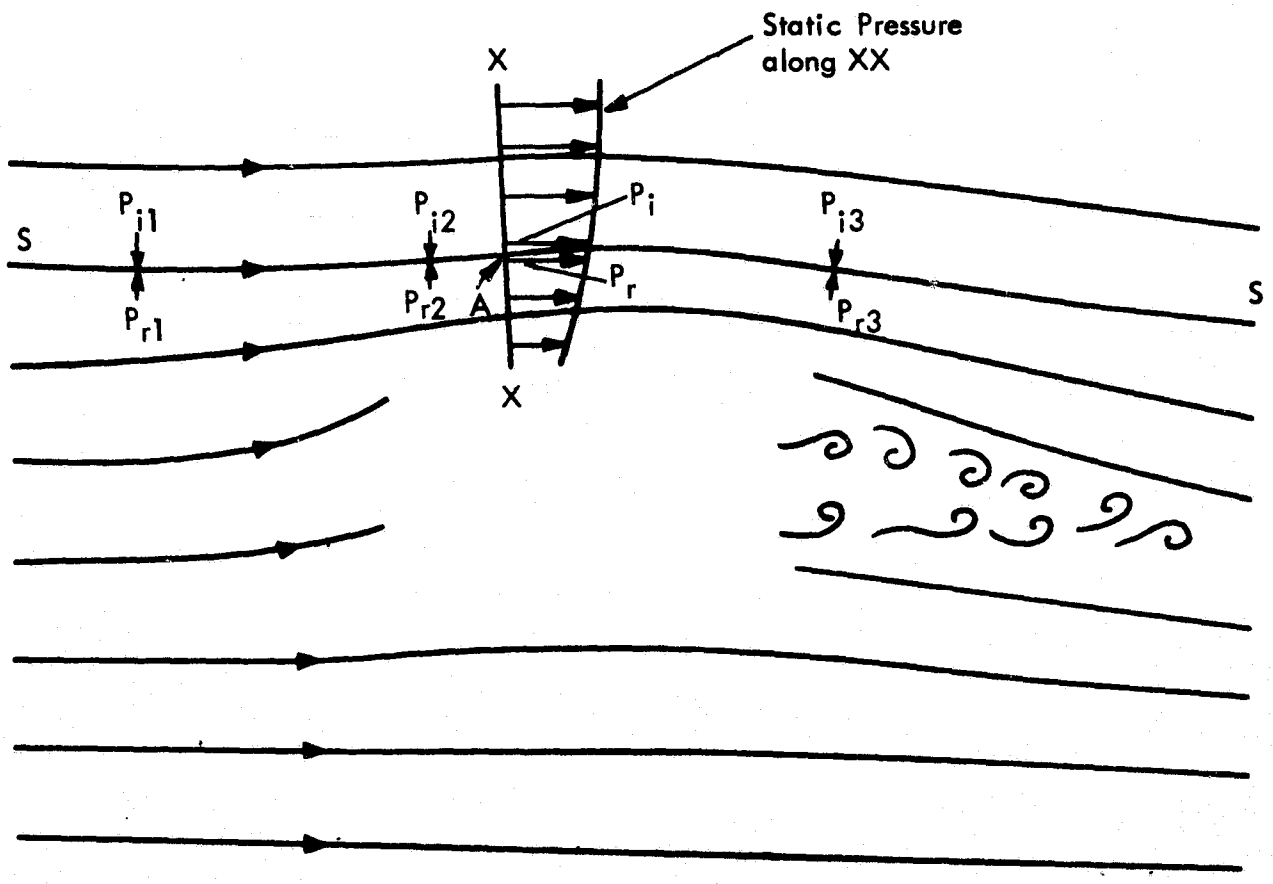

FIG.2. FREE AIR MODE STREAMLINE CRITERION: THE MATCHING OF REAL AND IMAGINARY PRESSURES ALONG THE TEST SECTION WALL STREAMLINE.

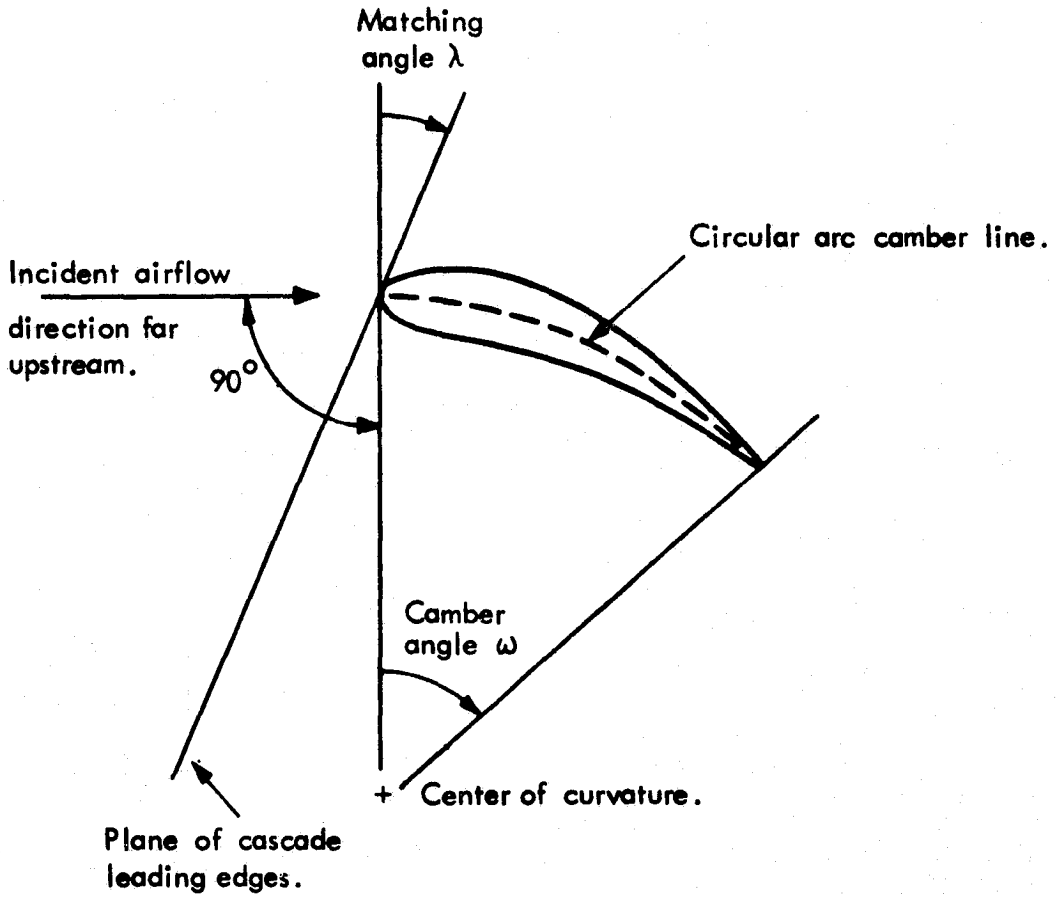

FIG.3. CASCADE GEOMETRY.

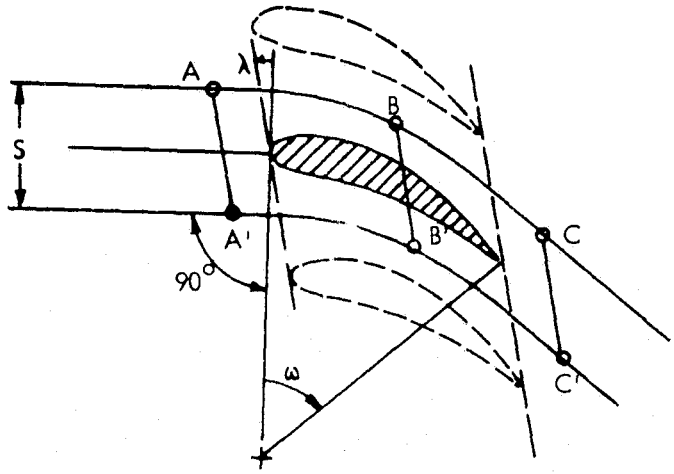

(a) Turbine cascade (λ is negative in this sketch.)

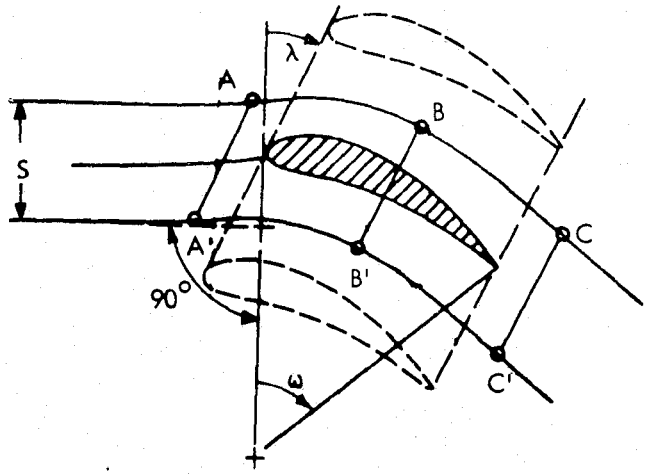

(b) Impulse turbine rotor cascade ($\lambda = \omega/2$.)

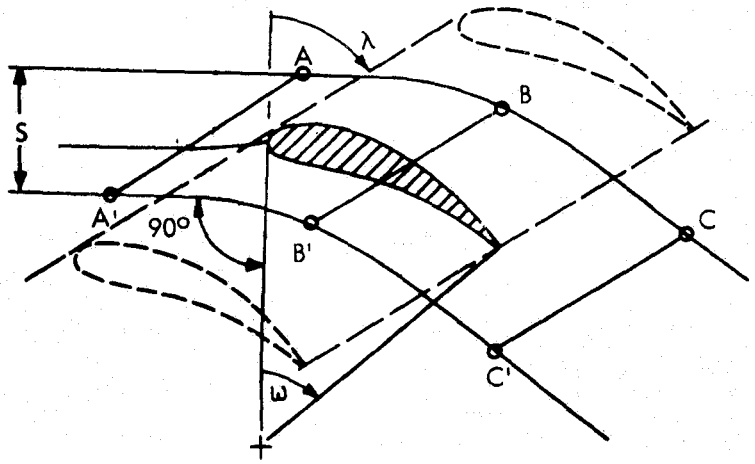

(c) Compressor cascade ($\lambda > \omega/2$.)

FIG.4. STREAMLINE AND TEST SECTION WALL GEOMETRIES FOR THE GENERATION OF TURBINE AND COMPRESSOR CASCADE FLOWS. STREAMLINES ABC, A'B'C' ARE SPACED ONE FOIL-PITCH APART THROUGHOUT AND ARE THE CONTOURS TO BE FOLLOWED BY THE FLEXIBLE WALLS.

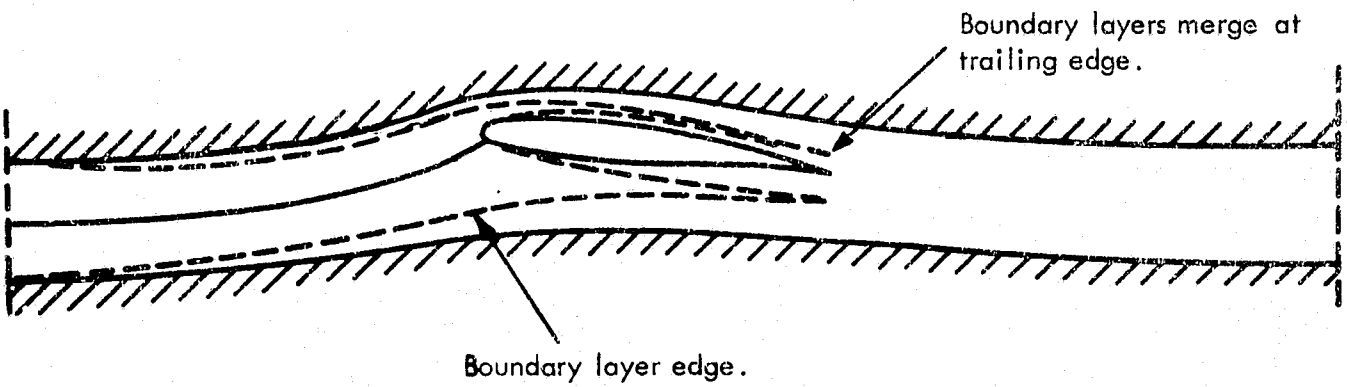

(a) Minimum depth as dictated by the merging of wall and wing boundary layers at the trailing edge.

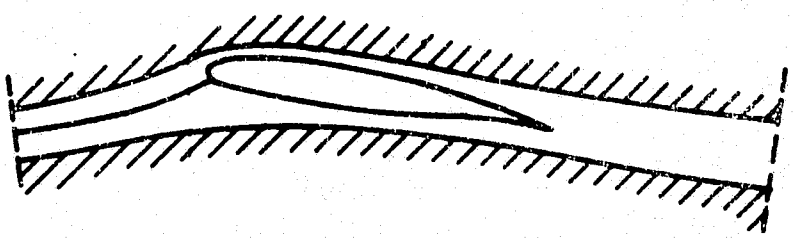

(b) Size reduction by truncation of length.

FIG.5. ILLUSTRATION OF POSSIBLE REDUCTIONS IN TEST SECTION SIZE.

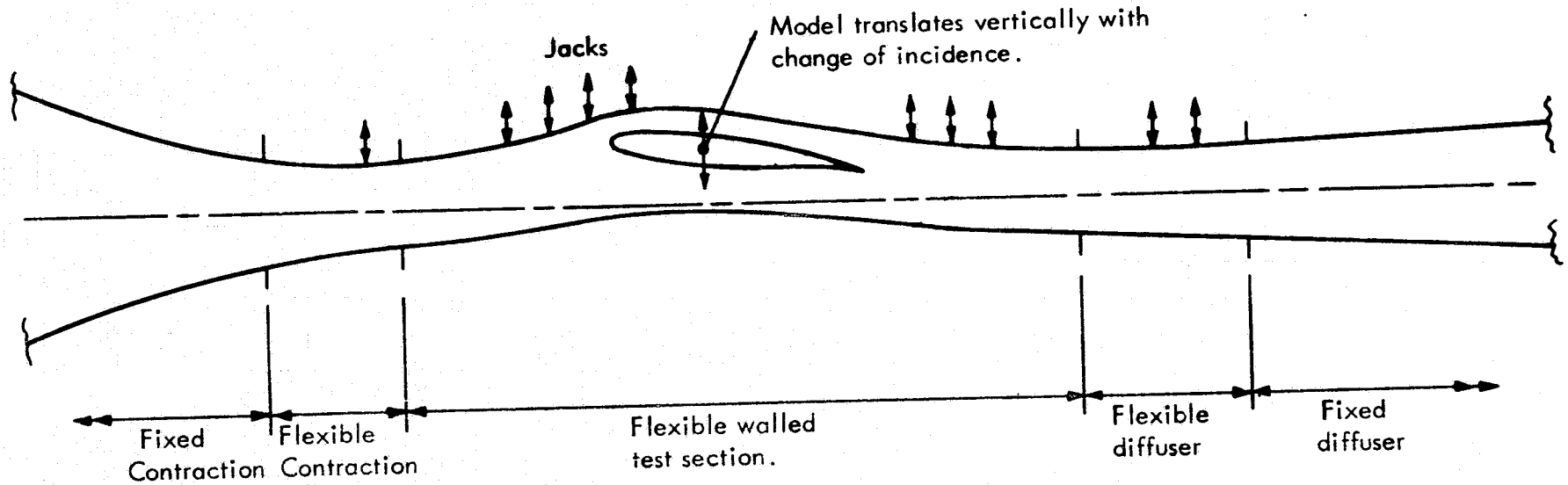

FIG.6. A TWO DIMENSIONAL SELF-STREAMLINING TEST SECTION DESIGN CONCEPT.

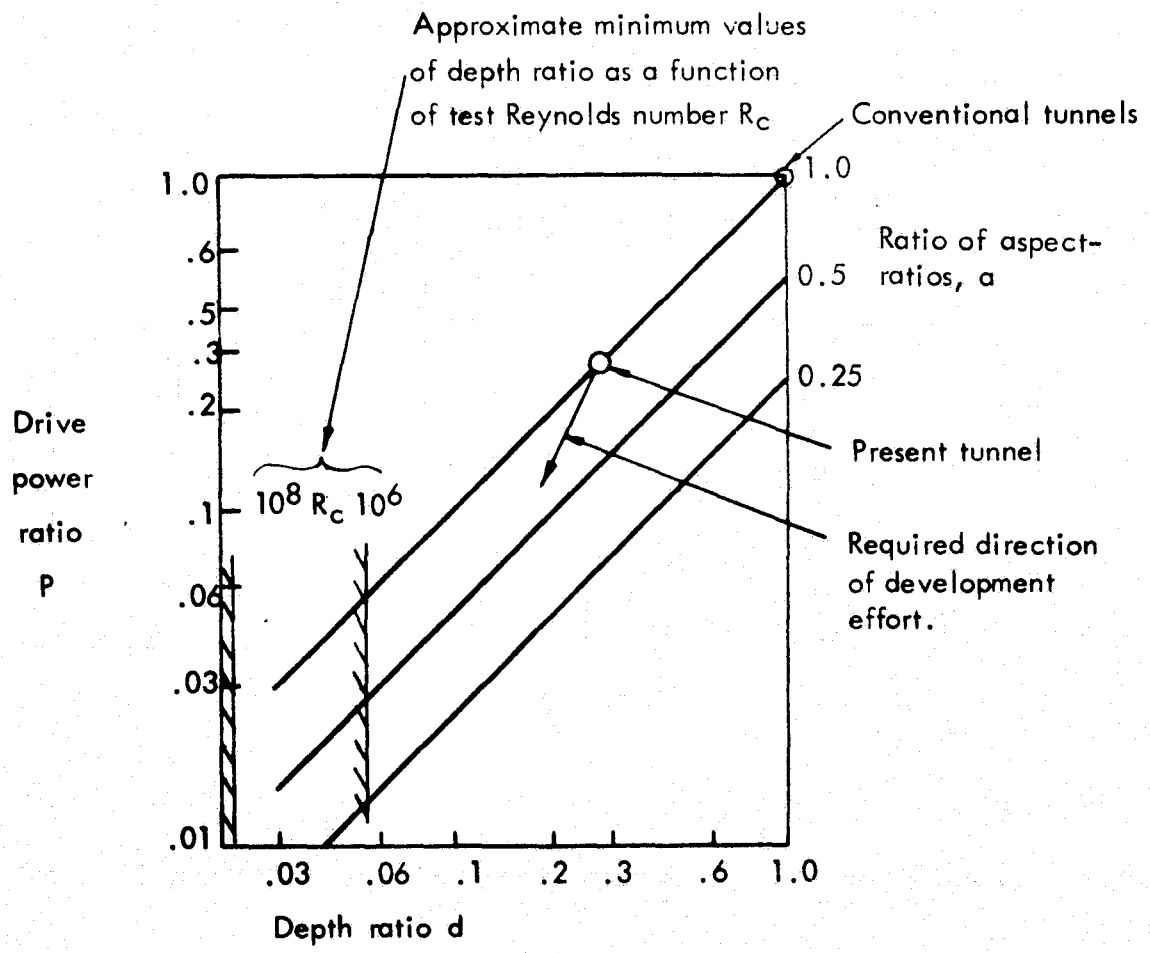

FIG. 7 . VARIATION OF TUNNEL DRIVE POWER WITH TEST SECTION GEOMETRY.

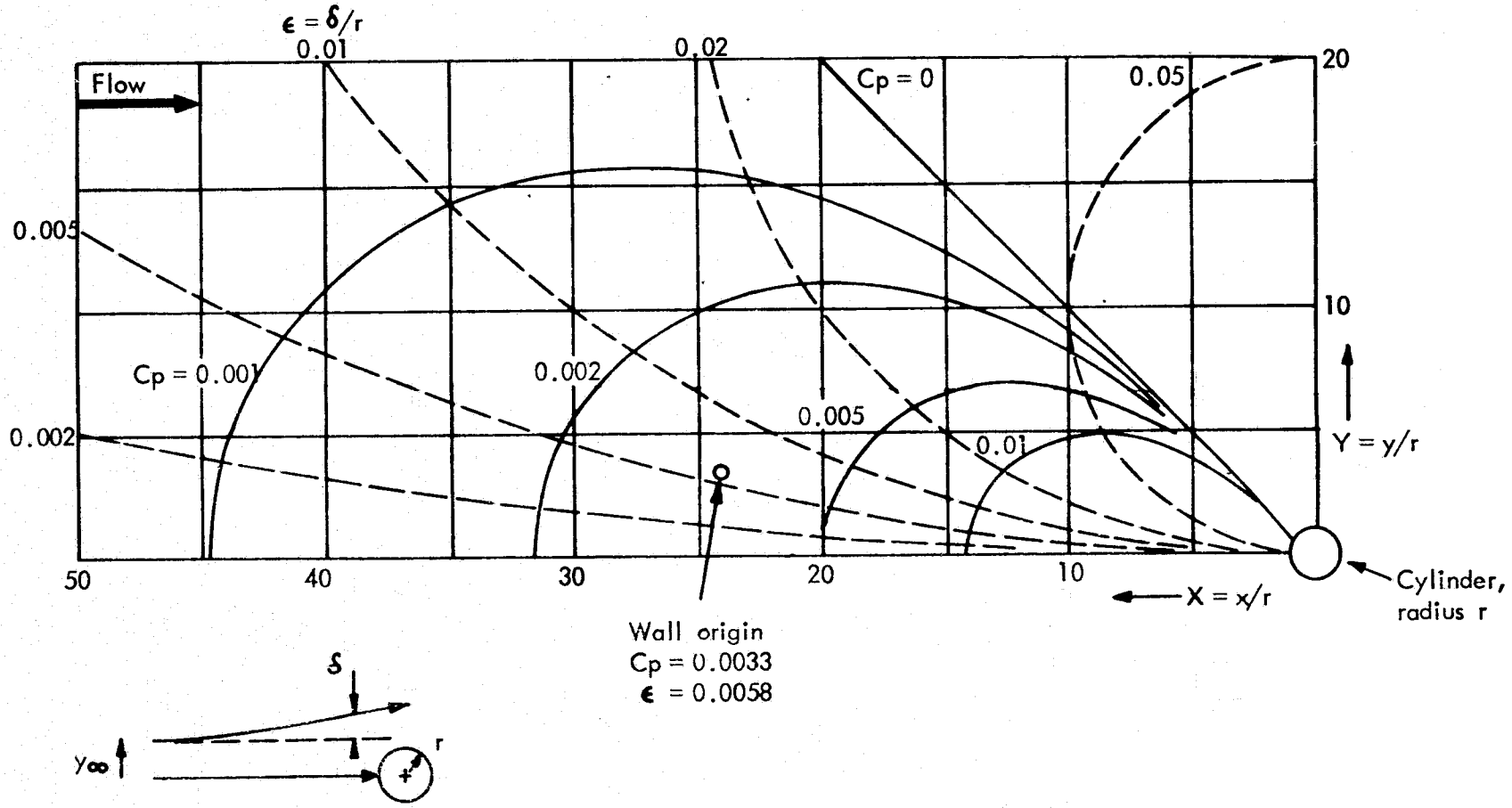

FIG.8. UPSTREAM INFLUENCE OF CYLINDER IN TWO-DIMENSIONAL POTENTIAL FLOW, IN TERMS OF STREAMLINE DISPLACEMENT AND PRESSURE FIELD.

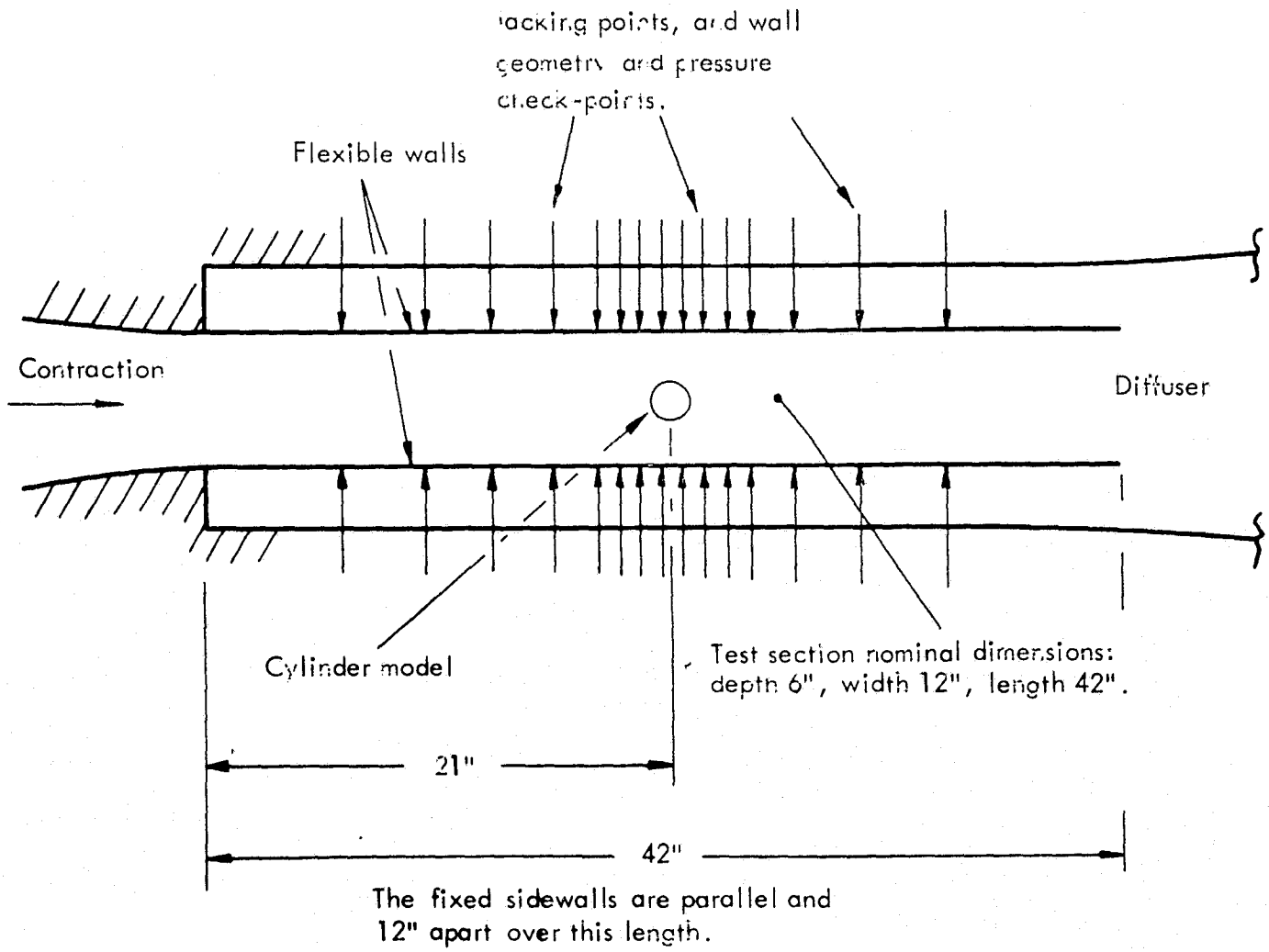

FIG. 9. TEST SECTION SIDE VIEW.

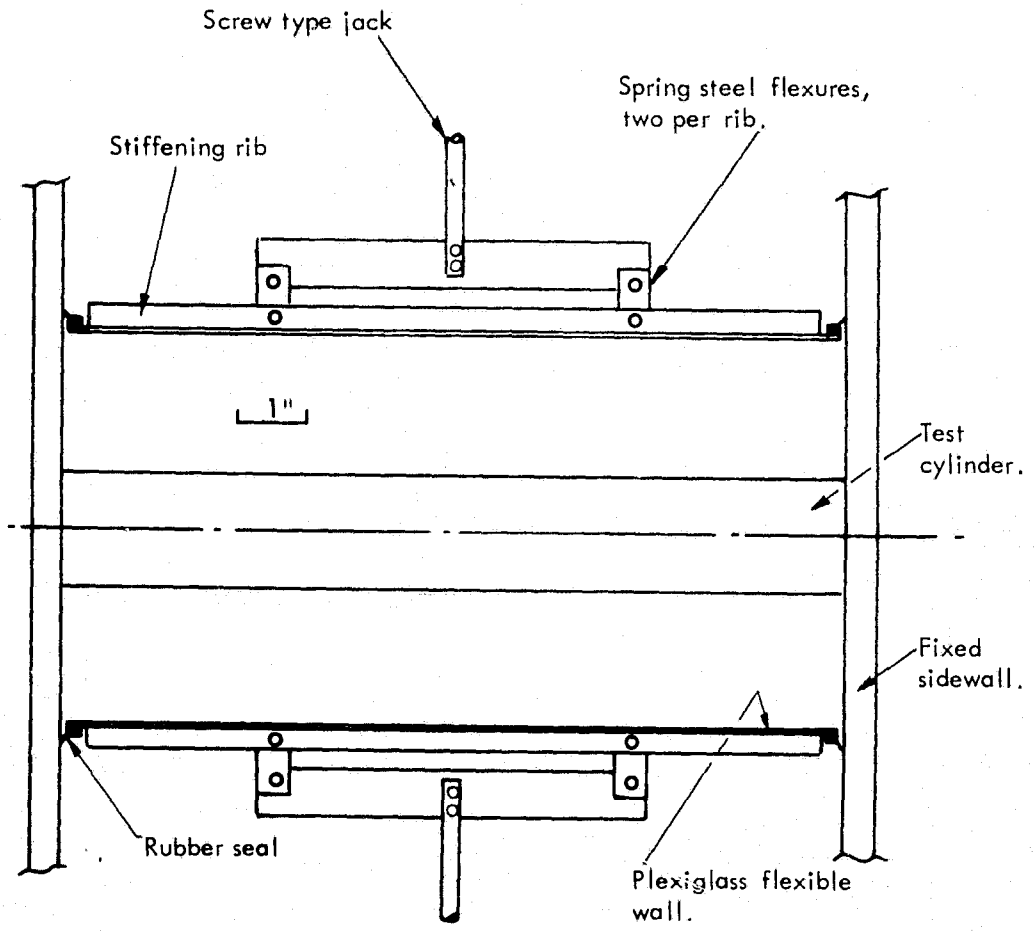

(a) View along test section, scale $^{1}/_{2.54}$.

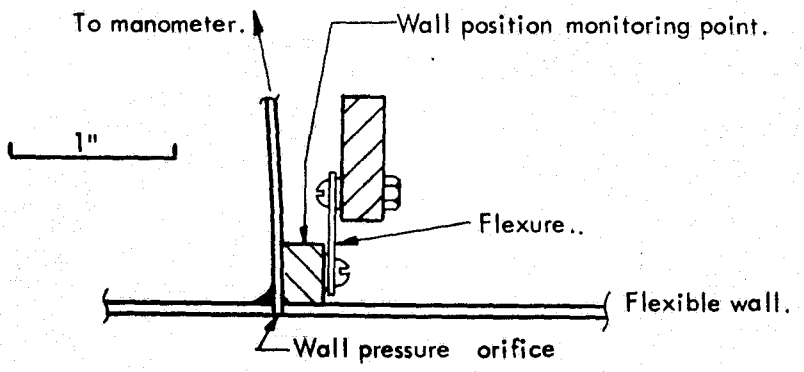

(b) Stiffening rib, flexure and pressure orifice details, full scale

FIG 10. SELF STREAMLING WIND TUNNEL. DESIGN DETAILS OF FLEXIBLE WALL TEST SECTION.

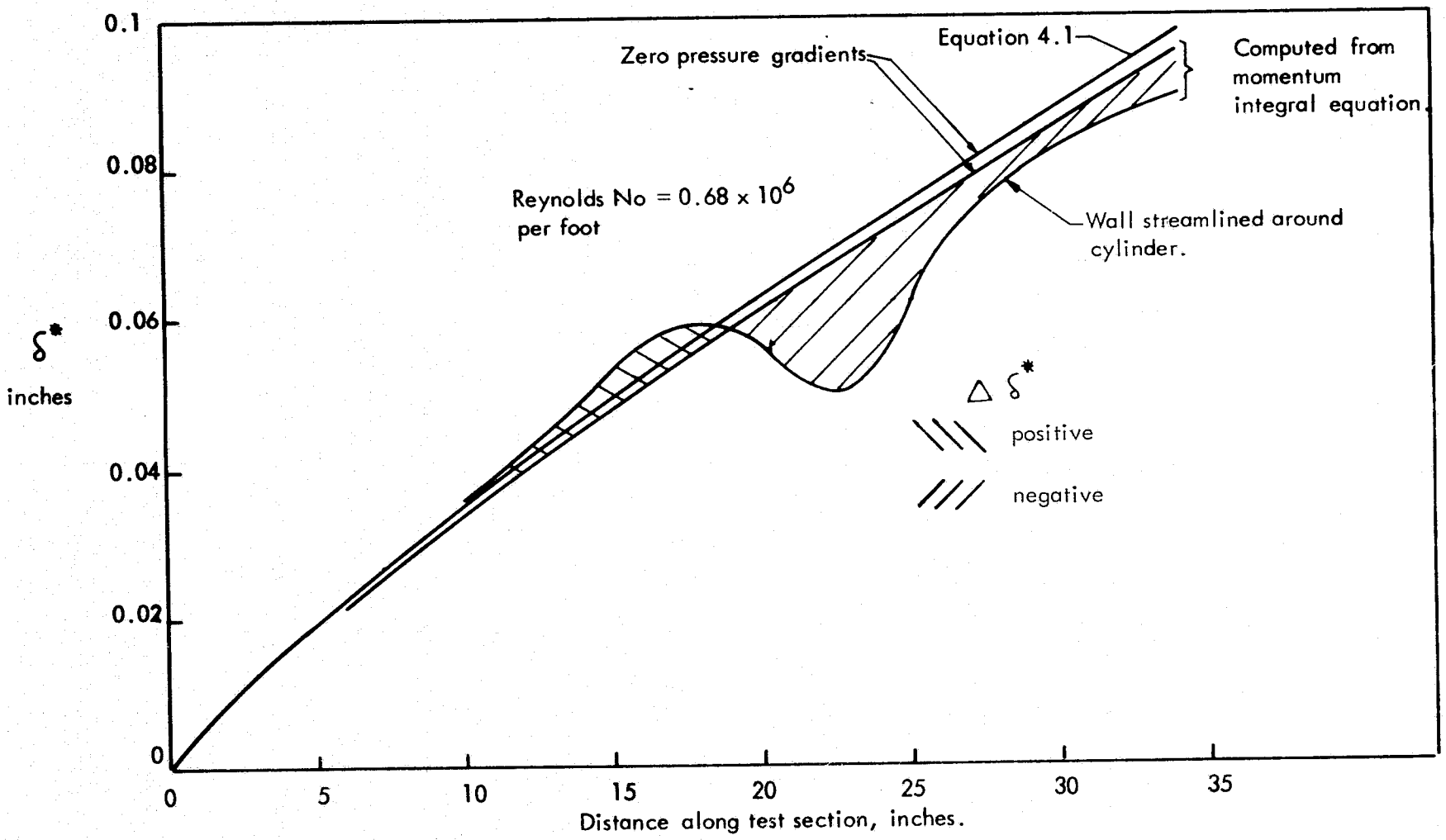

FIG. 11 EXAMPLES OF CALCULATIONS OF BOUNDARY-LAYER GROWTH ALONG THE TEST SECTION FLEXIBLE WALL.

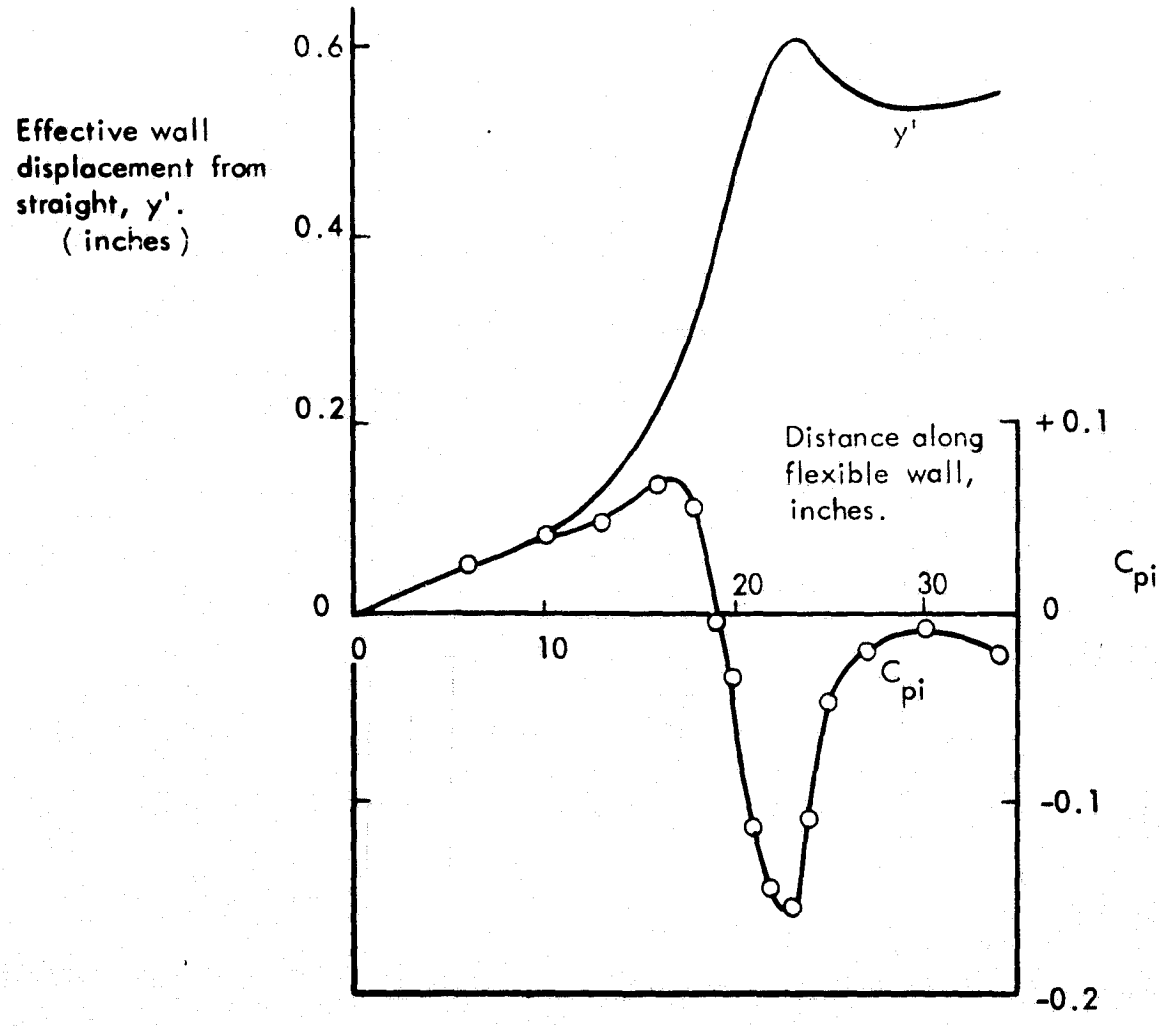

FIG . 12 A TYPICAL y' CONTOUR, WITH THE IMAGINARY FLOWFIELD SURFACE PRESSURE COEFFICIENT C_{pi} .

(a) The wind tunnel test.

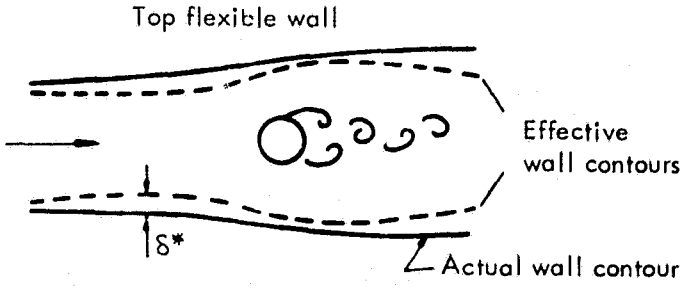

(b) Computer modelling of the imaginary flow field above the top wall, giving the shape of any streamline together with C_{pi}.

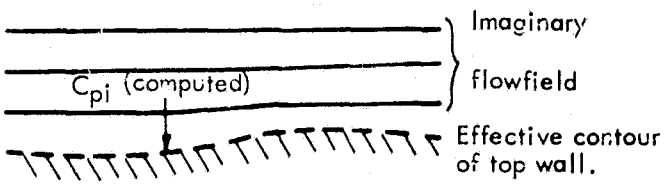

(c) Tunnel simulation of the portion of the imaginary flowfield adjacent to the real flowfield.

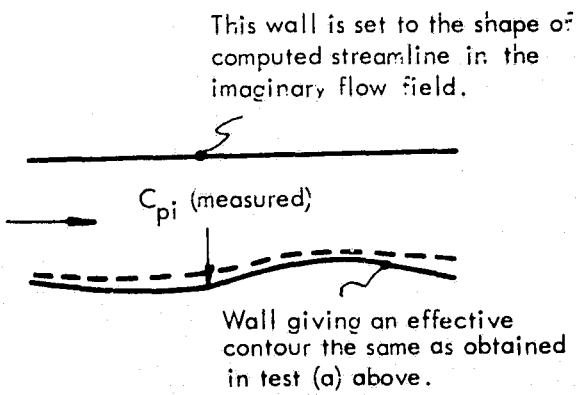

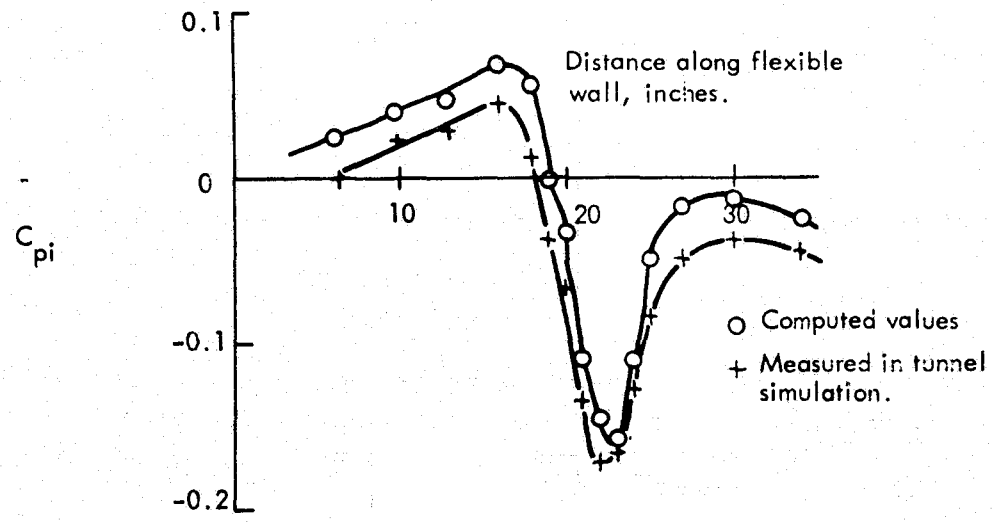

(d) The two pressure distributions.

FIG.13. A COMPARISON BETWEEN COMPUTED AND MEASURED PRESSURES ALONG THE IMAGINARY FLOWFIELD SIDE OF A TYPICAL WALL CONTOUR.

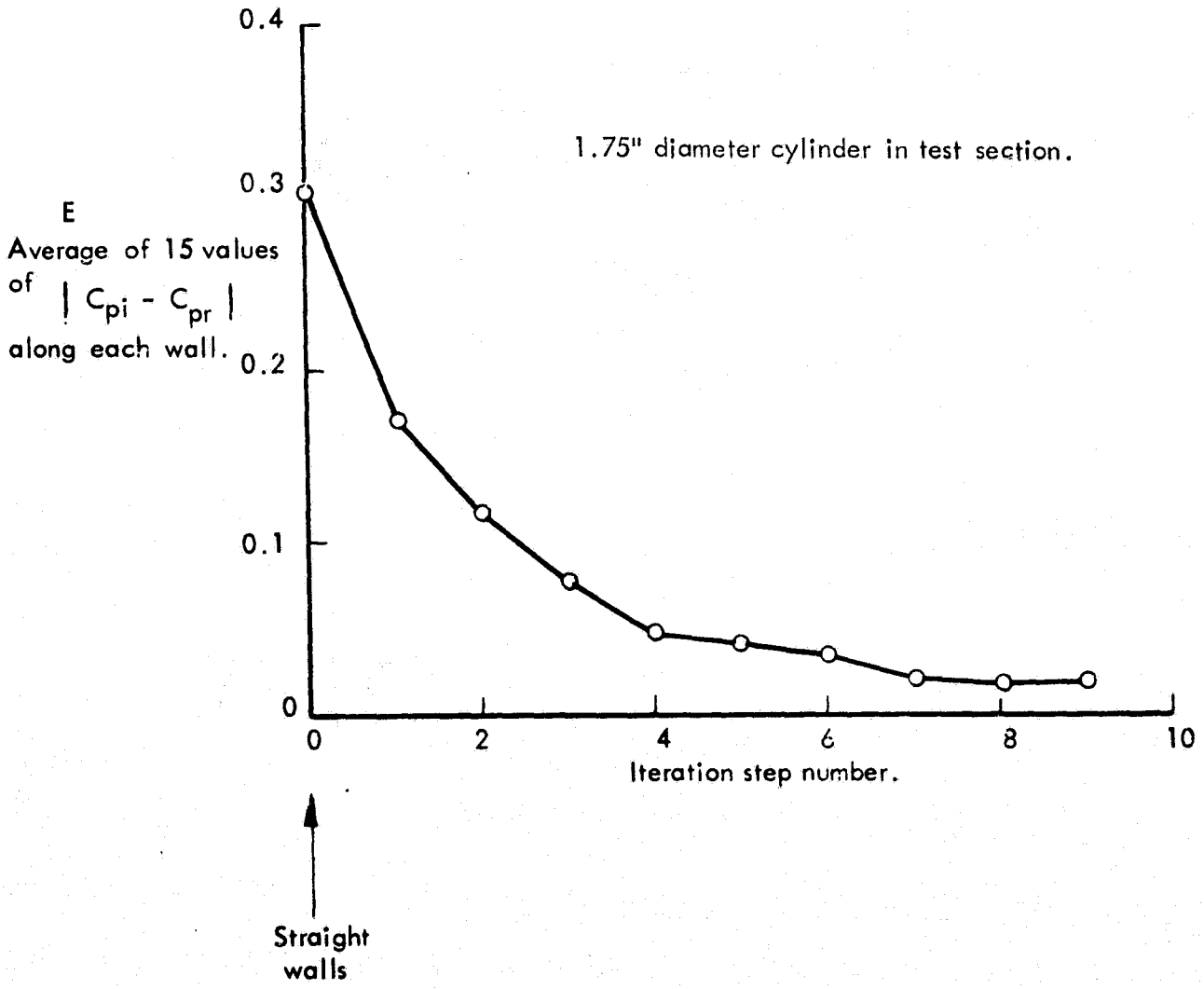

FIG .14. THE VARIATION OF A MEASURE OF THE PRESSURE IMBALANCE ACROSS THE WALL STREAMLINE DURING THE STREAMLINING PROCEDURE.

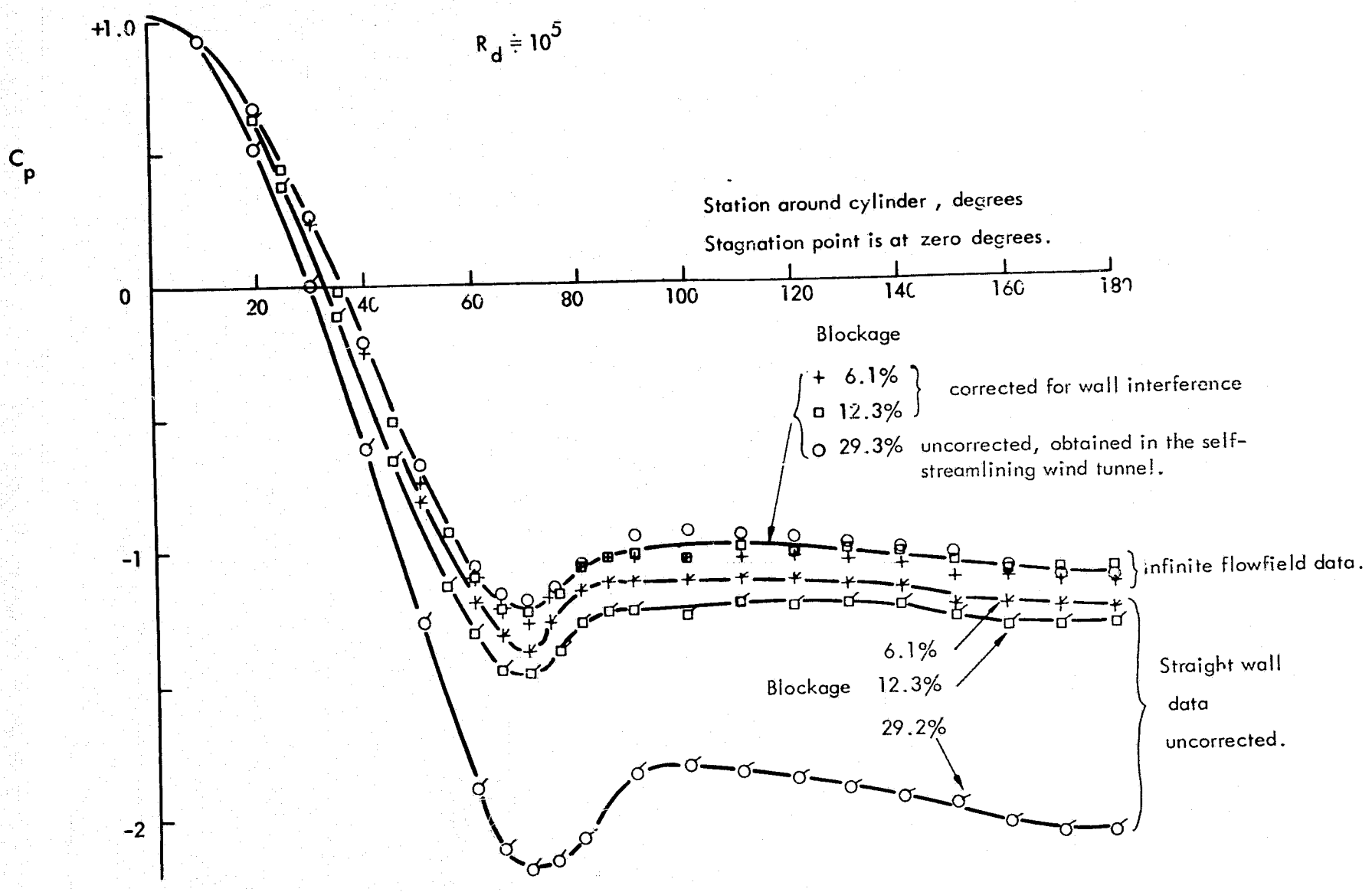

FIG. 15. COMPARISONS OF PRESSURE DISTRIBUTIONS AROUND CYLINDERS MEASURED IN STRAIGHT-WALLED AND STREAMLININED TEST SECTIONS.

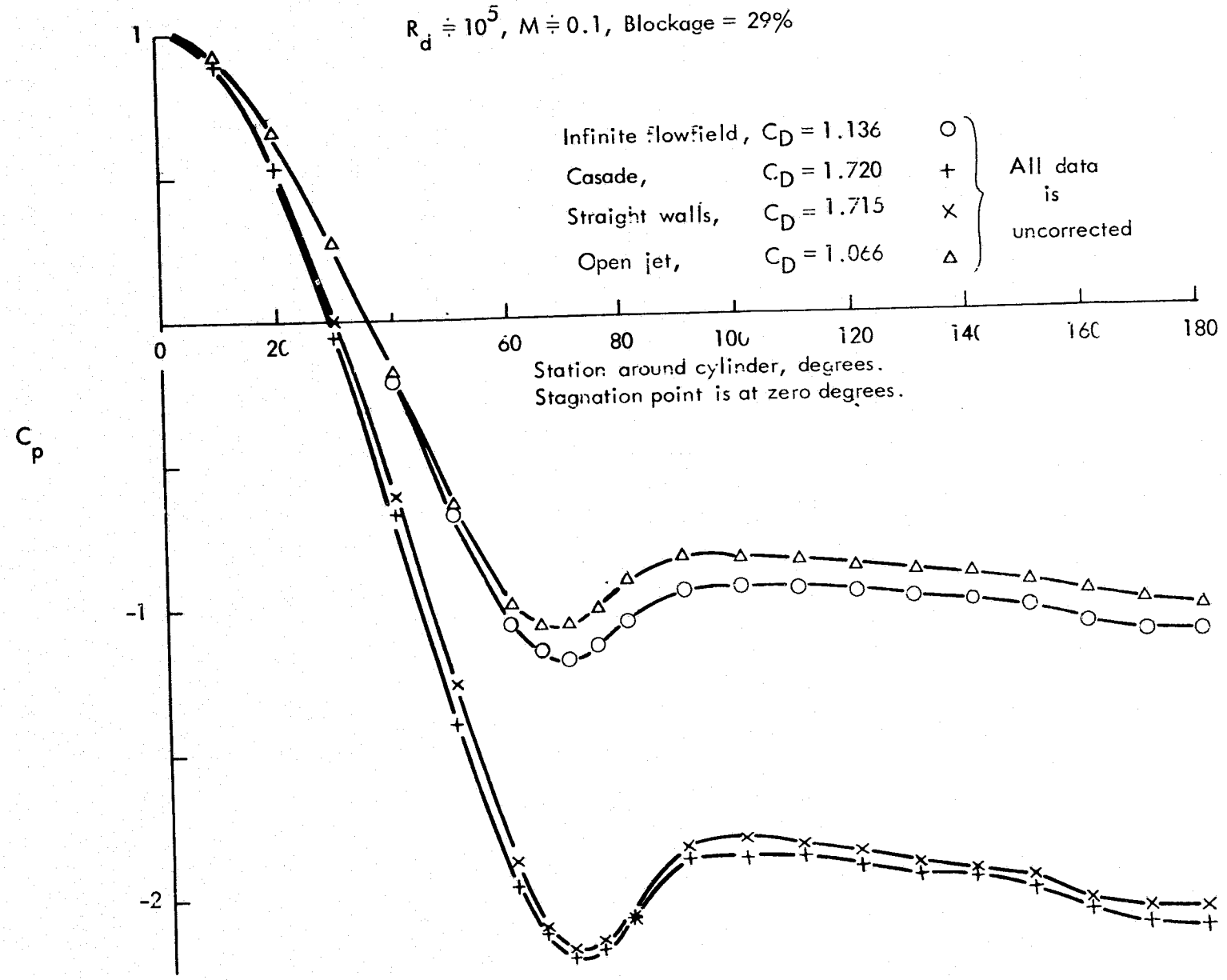

FIG. 16. CYLINDER PRESSURE DISTRIBUTIONS OBTAINED IN THE SELF STREAMLINING WIND TUNNEL IN SEVERAL OF ITS OPERATIONAL MODES.

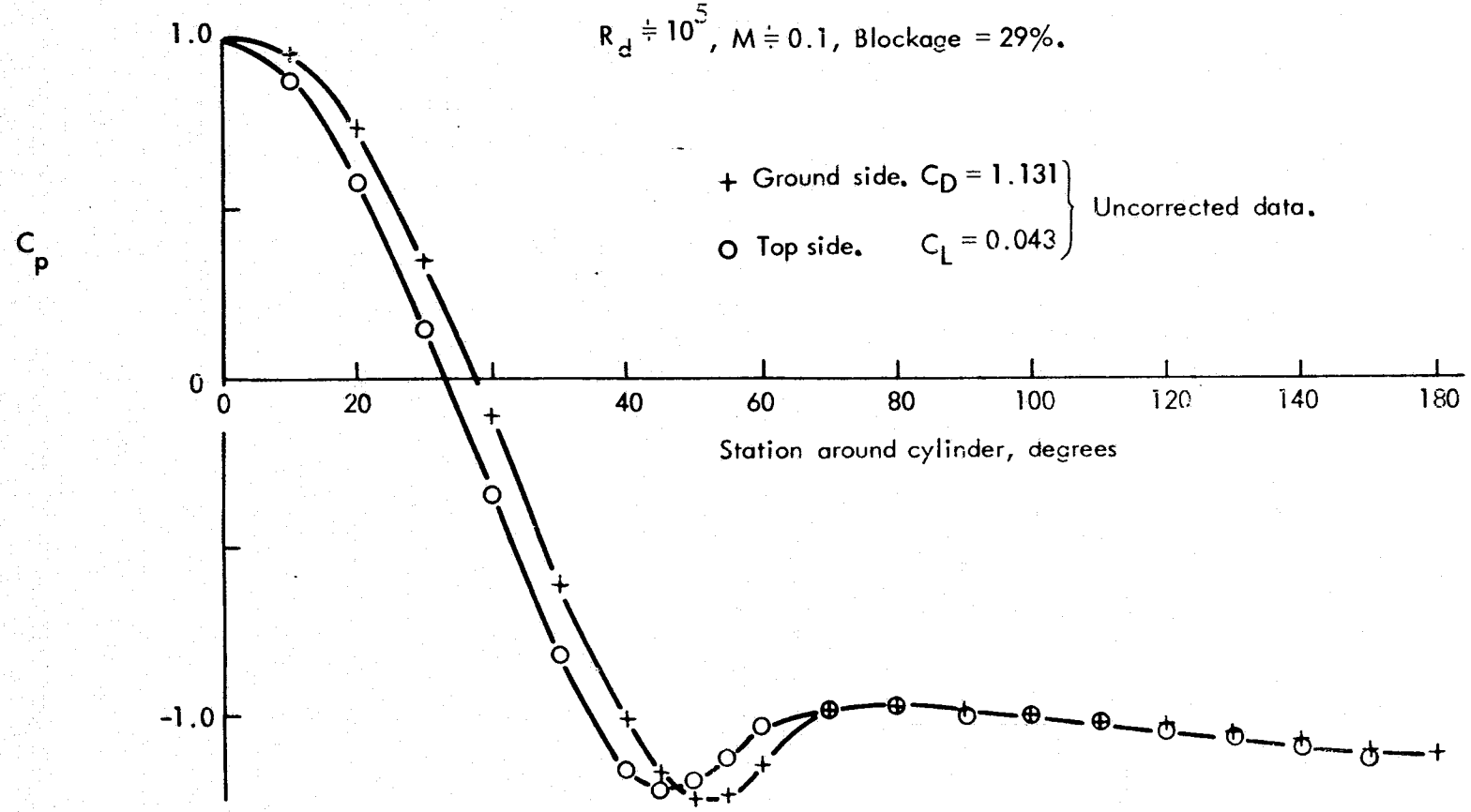

FIG. 17. CYLINDER PRESSURE DISTRIBUTION IN GROUND EFFECT.

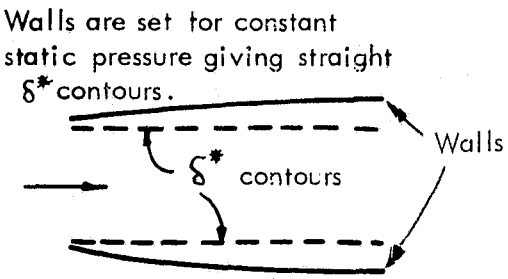

(a) Empty test section with "straight" walls.

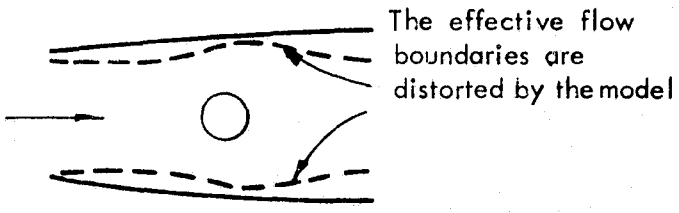

(b) "Straight" walls with model.

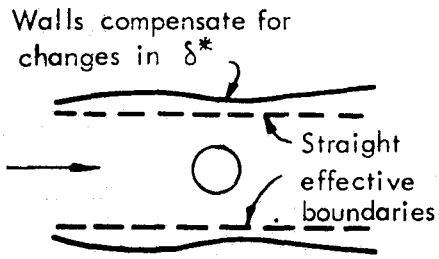

(c) Casade mode.

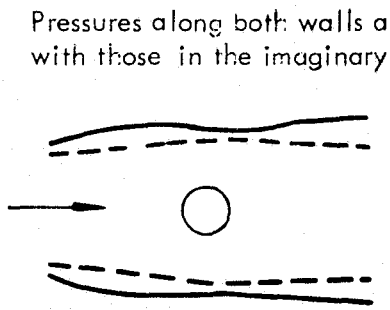

(d) Infinite flowfield mode.

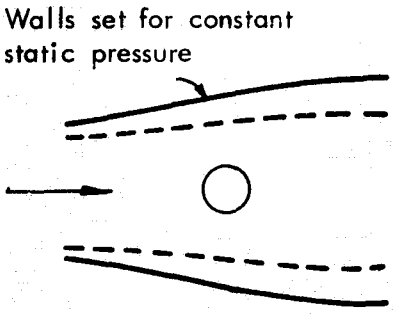

(e) Open-jet mode

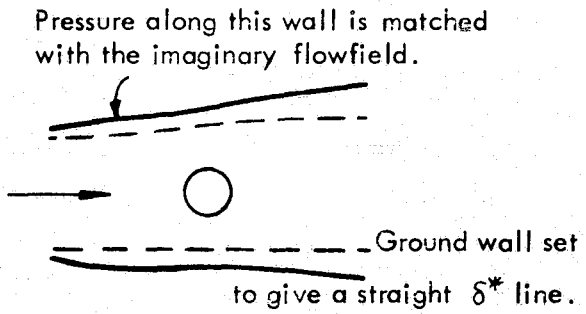

(f) Ground-effect mode.

FIG. 18. SKETCHES ILLUSTRATING THE VARIATIONS IN FLEXIBLE WALL SHAPES AND δ^* CONTOURS BETWEEN SEVERAL MODES OF OPERATION OF OF THE SELF STREAMLINING WIND TUNNEL.

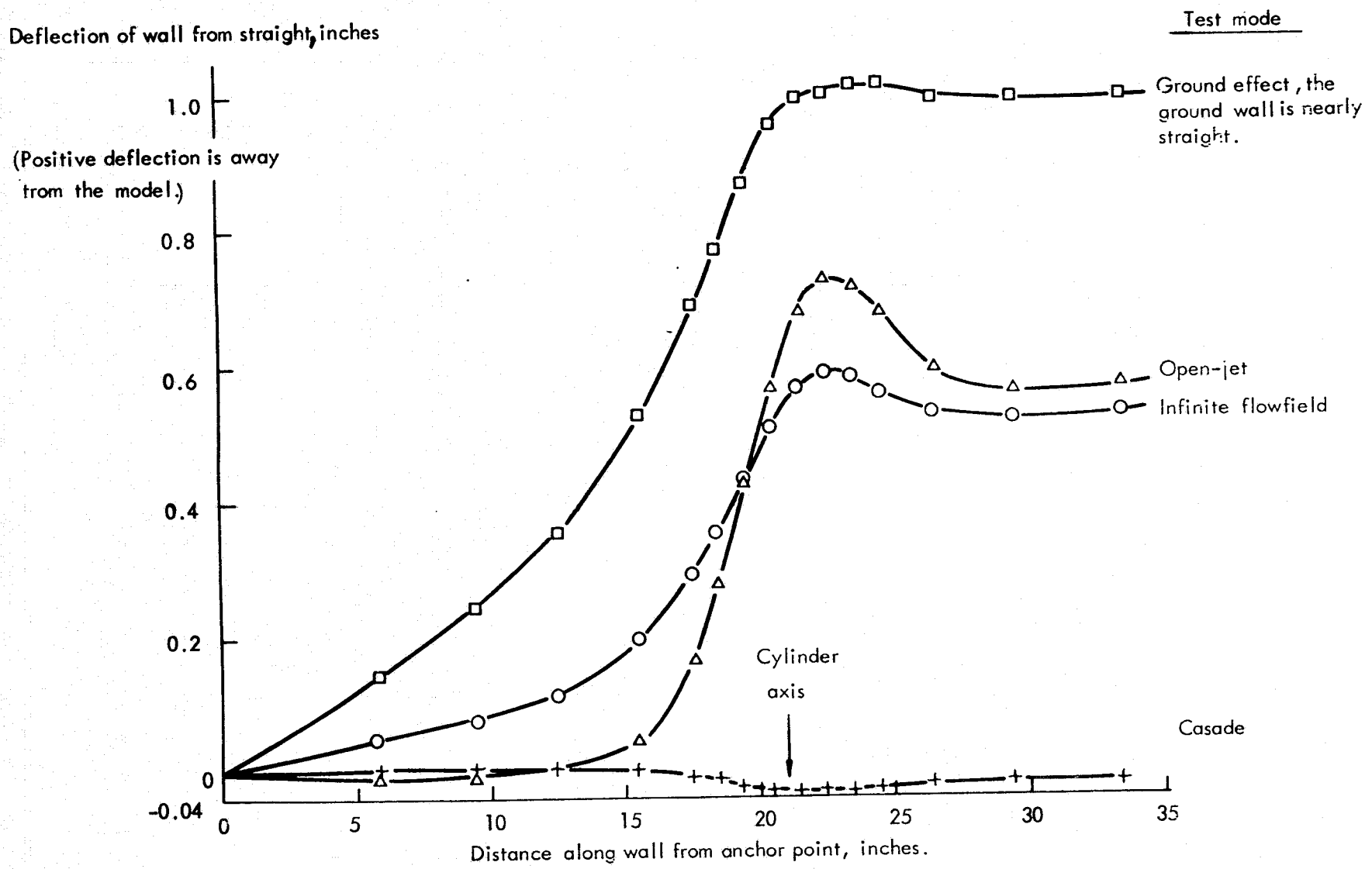

FIG. 19. CONTOURS ADOPTED BY THE WALLS OF THE SELF STREAMLINING WIND TUNNEL, AT THE CONCLUSIONS OF THE ITERATION PROCESSES FROM STRAIGHT SETTINGS, FOR SEVERAL MODES OF OPERATION.